NASA CR-112035

PROPELLANT SIDEFEED-SHORT PULSE DISCHARGE THRUSTER STUDIES

by

Dominic J. Palumbo
and
William J. Guman

January, 1972

PCD-TR-72-1, FHR 4031A, PC004R9401

Prepared under Contract NAS 1-10944
Fairchild Industries, Inc.
Fairchild-Republic Division
Farmingdale, New York 11735

for

National Aeronautics and Space Administration
LANGLEY RESEARCH CENTER
Langley Station
Hampton, Virginia 23365

NASA CR-112035

PROPELLANT SIDEFEED-SHORT PULSE DISCHARGE THRUSTER STUDIES

by

Dominic J. Palumbo
and
William J. Guman

January, 1972

PCD-TR-72-1, FHR 4031A, PC004R9401

Prepared under Contract NAS 1-10944
Fairchild Industries, Inc.
Fairchild-Republic Division
Farmingdale, New York 11735

for

National Aeronautics and Space Administration
LANGLEY RESEARCH CENTER
Langley Station
Hampton, Virginia 23365

FOREWORD

This final report summarizes the work performed under contract NAS-10944 for National Aeronautics and Space Administration, Langley Research Center, Hampton, Virginia. The effort was accomplished under the direction of Mr. J. M. Hoell of NASA, Langley.

Dr. W. J. Guman was the Principal Investigator with Dr. D. Palumbo a principal contributor to the results of this study. The laboratory effort was performed with the assistance of Messrs. W. Johnson, E. Poggi and A. Scheiweiller. The constructive discussions with Mr. Hoell are gratefully acknowledged.

ABSTRACT

The technique of feeding a solid propellant into the discharge from the sides of the discharge was evaluated. The thrust/power ratio could in cases be significantly effected by the included angle of V-shaped propellants and by the electrode length. This result implies that when results are compared at the same specific impulse it is possible to obtain higher thrust efficiencies. In particular, it was found that for a given discharge energy the thrust/power ratio correlated with propellant mass. Increasing the integral $\int i^2 dt$ simultaneously increases both the gasdynamic and electromagnetic thrust. An analytic expression was formulated for ablated mass which comprehensively describes experimental data in terms of geometry and electrical parameters. The previously reported correlation of the product impulse x specific impulse with discharge energy has also been analytically described. Tentatively it is concluded that the reliability of dry energy storage capacitors does not equal the reliability of liquid impregnated units when the comparison is made at the same joules/Kg rating.

CONTENTS

ILLUSTRATIONS

ILLUSTRATIONS (Cont'd)

SECTION I

INTRODUCTION

Modern space mission objectives have become increasingly dependent upon accurately positioning and orienting either orbiting satellites or inter-planetary spacecraft. For this reason considerable emphasis has been placed on developing a pulsed plasma electric propulsion system. Such a propulsion system can either provide an equivalent steady state thrust in the micropound and millipound regimes or repeatedly provide sharply defined impulse bits of known amplitude at high values of specific impulse.

Among the various criteria used for assessing the relative usefulness of an electric propulsion system for a particular mission, the characteristic thrust-to-power ratio (or the specific thrust) is a parameter of considerable importance. This parameter determines whether or not the thrust levels required for a particular mission can be produced by the thruster with the available on-board power. The thrust-to-power ratio of a pulsed plasma propulsion system will also have a direct effect on the weight of the propulsive system since the energy storage capacitors, which are prime components, will increase in weight as the required discharge energy increases. Isolated data reported in a previous program (1) revealed that it should be possible to realize a significant increase in the thrust/power ratio by providing propellant from the sides of the discharge. The major effort of this program has, therefore, been directed at a systematic study for increasing the thrust-to-power ratio of the solid propellant pulsed thruster and to determine the physical parameters that govern this ratio. The experimental work performed during this program was in the millipound thrust regime and limited to discharge energies of 300 and 500 joules.

It should be noted that this program was primarily concerned with a determination of the parameters and an understanding of the factors governing the thrust/power ratio. No attempt was made to optimize thruster efficiency. Thus, any comparison of efficiency as reported herein with other thrusters should be made at the same value of specific impulse.

Electrode erosion was also examined during this study and results are presented in Section VII.

Concurrent with the aforementioned studies, two 300 joule energy storage capacitors were procured from Capacitor Specialists Inc. (CSI) and experimentally evaluated for their applicability as an energy storage source. The capacitors were of a dry construction (no liquid impregnant) using Kapton as the dielectric and rated at about 10 joules/lb. The result of this capacitor evaluation is presented in Section VIII of this report.

SECTION II

THRUSTER DESCRIPTION

Most of the studies being reported upon were performed with the basic short pulse discharge thruster reported in Reference 1. This latter thruster is comprised of two aluminum disk shaped current collector plates (anode and cathode) separated by a dielectric. Up to twelve energy storage capacitors can be connected to these collector plates thereby forming a relatively low inductance discharge circuit. The anode and cathode of the electrode nozzle assembly are attached to the respective positive and negative collector plates. These plates have appropriate cutouts to allow fastening of the electrodes. Figure 1 shows a typical rear view of the assembly whereas Figure 2 presents a front view showing the V-shaped teflon propellant located between a parallel rail accelerator nozzle. The discharge current flows in a radial direction from the capacitors, to the electrodes through the arc, and back to the capacitors.

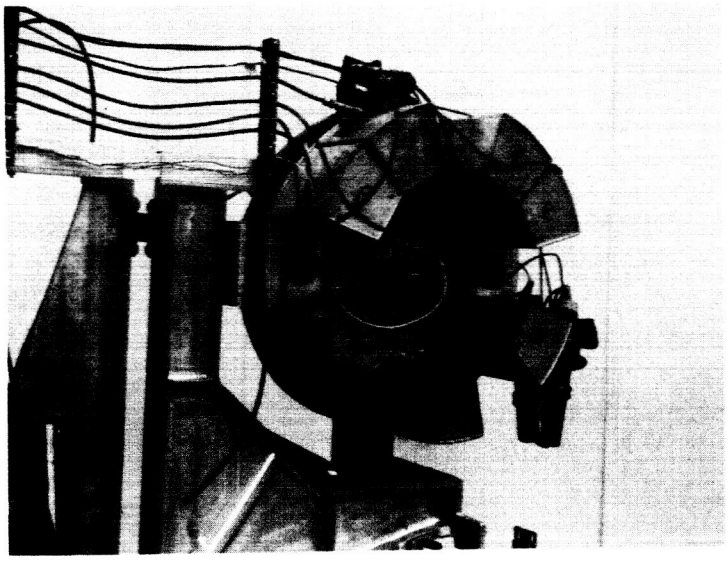

Figure 1. Rear View of 300 Joule Capacitor Short Pulse Test Bank Mounted on Thrust Balance

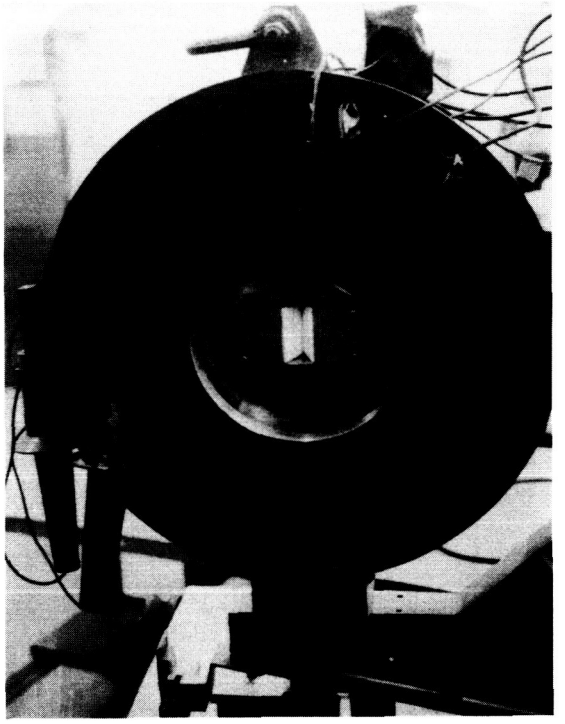

Figure 2. Front View of Thruster with V-shaped Propellant

Conceptually the thruster is schematically represented as shown in Figure 3.

The propellant used is virgin TFE teflon. Various geometric configurations for the electrode-propellant assembly have been examined in the past. This research was performed using a parallel rail electrode configuration with propellant being fed in from either side of the interelectrode gap. This geometry is illustrated in Figure 4. The front face of the teflon fuel rods are shielded from the plasma using Mykroy to insure that only the teflon surfaces of the V are exposed. All exterior electrode surfaces are insulated with a coating of epoxy cement.

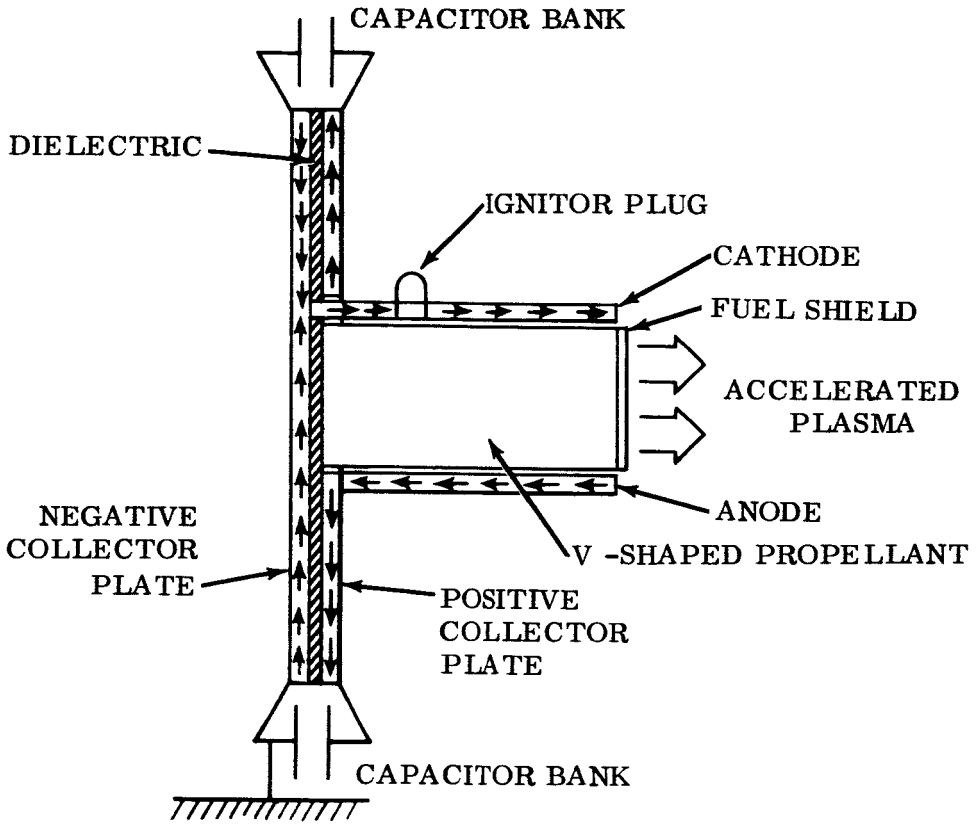

Figure 3. Thruster Schematic

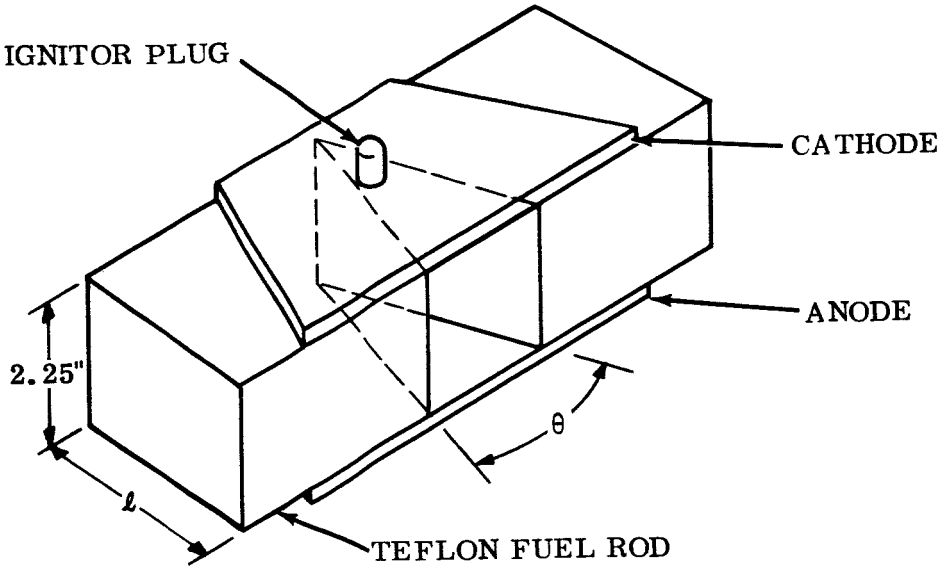

Figure 4. Schematic of Side-Fed Electrode-Propellant Configuration

The parameters that were varied during the performance evaluation studies include the electrode length ℓ and the included angle θ between propellant surfaces. Variations in thruster performance as a function of these parameters were recorded and results are presented in Section V of this report.

A photo of a typical fuel assembly and electrodes taken after a test is included below in Figure 5.

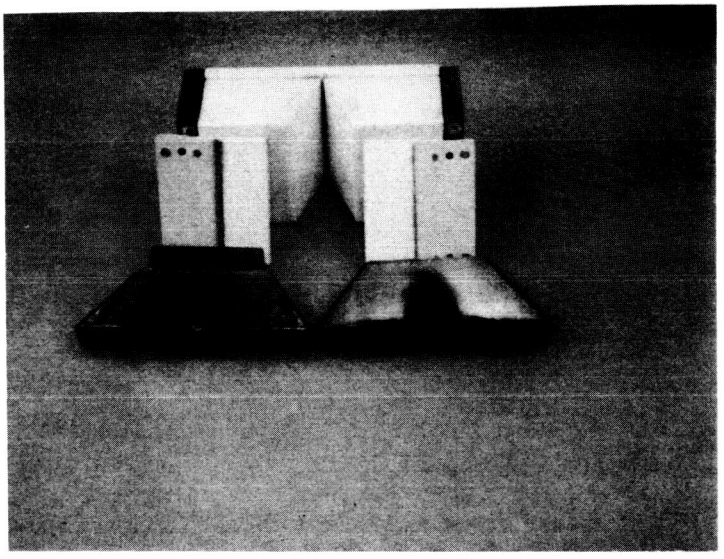

Figure 5. Typical Electrode - Propellant Components After 3500 Shots.

SECTION III

THRUSTER PERFORMANCE EVALUATION

In order to evaluate thruster performance it was necessary to directly measure:

a) Thrust
b) Impulse Bit Amplitude
c) Pulse Frequency
d) Propellant Mass Per Discharge
e) Eroded Mass Per Discharge
f) Discharge Current Variation
g) Discharge Voltage Variation
h) Initial Capacitively Stored Energy

Details of how these parameters are experimentally measured and the equipment that was used to perform the measurements are described in Reference 1.

Each set of performance data presented in this report was obtained through the laboratory procedure briefly described below:

(1) Weigh the propellant and electrodes individually to within ± 0.2 milligram.

(2) Mount the engine on the thrust balance and place it in the vacuum chamber. Evacuate the chamber to about .05 microns (5×10^{-5} mm Hg).

(3) Fire the engine for approximately 200 consecutive discharges to remove any mass absorbed on the propellant and electrode surfaces while they were exposed to atmospheric conditions.

(4) Take three thrust balance ball calibration readings and three thruster thrust level readings. Take photographs of oscilloscope traces of thruster discharge current and voltage and a true ground reading. Measure discharge pulse rate.

(5) Repeat Step (4) at 1000, 2000, and 3000 consecutive shots.

(6) Allow engine to cool in vacuum and then remove it from the vacuum chamber. Reweigh propellant and electrodes individually.

Each of the four sets of thrust data readings (i.e., at 200, 1000, 2000, and 3000 discharges) are reduced separately by averaging the three amplitudes of the ball calibration waveforms and thruster waveforms and using these averages to compute the thrust. Test average thrust (T) is computed as the average of these

four values. Generally these four values are within ±5% of the test average value (See Reference 1). The four recorded discharge frequencies (f) are averaged and the impulse bit (I) is calculated, from the relation $I = T/f$.

The test average energy initially stored in the capacitor (E_o) is computed from the average value of the initial voltages recorded on the oscilloscope photographs obtained during the performance test. The test average power (P) consumed is then equal to the test average pulse frequency multiplied by the test average initial energy. The thrust-to-power ratio is then computed from the ratio of test average thrust to test average power.

As described in Reference 1, the propellant mass per discharge (m_d) used in performance calculations is the test average change in initially stored propellant mass. No corrections are applied for mass utilization efficiency.

The test average specific impulse (I_s) is calculated from the ratio of test average impulse bit (I) to the test average propellant mass per discharge. Thruster efficiency $\eta = T^2/2\dot{m}P = I^2/2\, m_d E_o$. In this study no corrections were applied for mass utilization efficiency or energy transfer efficiency in presenting thruster efficiency.

One of the oscilloscope photographs of a given test is used to determine the discharge current (i) and voltage (v) as a function of time. The product of i and v is then tabulated with the time and numerically integrated to determine the energy delivered to the electrodes. Energy transfer efficiency η_E, for the discharge being examined is then computed from the relation $\eta_E = 1/E_o \int_o^\infty i(t)\, v(t)\, dt$ with E_o based on the initial voltage of that particular recording on the same photograph.

SECTION IV

PERFORMANCE DATA AND ANALYSIS

Performance data on rail-electrode V-shaped propellant configurations, as illustrated in Figure 4, were obtained for electrode lengths of 5.72 cm (2.25"), 4.09 cm (1.61"), 3.17 cm (1.25") and 2.28 cm (0.9") and included propellant angles of 0°, 40°, 60°, and 80°. All but two tests were performed at initial energies of approximately 300 joules. The interelectrode spacing was 5.72 cm (2.25") in all cases. The results of these tests are presented in tabular form in Table 1 of this report. A discussion of the results is presented below.

4.1 THRUST/POWER RATIO AS A FUNCTION OF GEOMETRY

The thrust-to-power ratio is presented in Figure 6 as a function of electrode length for the various included angles of the V-shaped propellant configurations considered. As indicated by this figure, the thrust/power ratio was found to be virtually independent of included angle θ at electrode lengths 0.90 in. and 2.25 in. In contrast, a wide variation in the thrust/power ratio with included angle was found at an electrode length of 1.60 in. Furthermore, it was observed that values of thrust/power ratio are maximum for all three angles examined at this particular length. Hence, it appears that for the conditions examined, a length of 1.60 in. provides the largest thrust-to-power ratio. Because of the rather large spacing between the data points, an additional test using an electrode length of 1.25 in., and included angle of 40° was performed to determine whether or not the optimal length could possibly be located between electrode lengths from 0.90 in. to 1.60 in. The test performed with the 1.25 in. electrode produced a thrust-to-power ratio of 5.84 μ lb/watt as compared to 6.04 μ lb/watt at an electrode length of 1.60 in. An exploratory test with an electrode length between 1.60 in. and 2.25 in. was not carried out. The possibility also exists that there could be an optimal length associated with each different included angle. While it would be interesting to resolve these questions, a comprehensive optimization of thrust/power with respect to all of these parameters was beyond the scope of the program. To the best of our knowledge, for the conditions examined, an electrode length of 1.60 in. provided the largest thrust-to-power ratio that could be obtained. Because of the increase in T/P

TABLE I. RESULTS OF 300 JOULE PERFORMANCE TESTS ON SIDE-FED CONFIGURATIONS

Log Number	135-4	135-5	135-6	135-7	135-8	135-9	135-12	135-13	135-14	135-19
Electrode Length, ℓ (inches)	1.6	1.6	1.6	1.6	2.25	2.25	0.9	0.9	0.9	1.25
Included Angle, θ (degrees)	80	40	60	0	60	80	60	80	40	40
Total Number of Shots, N	3538	3219	3064	3151	3100	3371	3112	3119	3124	3119
Capacitance, C (μfd)	67.4	67.4	67.4	67.4	67.4	67.4	67.4	67.4	67.4	67.4
Initial Voltage, V_o (KV)	2.90	2.97	2.96	2.96	3.00	2.99	2.95	2.89	2.99	3.03
Initial Energy, E_o (Joules)	284	298	297	295	303	302	294	282	302	308
Thrust, T (μ lb)	1038	1182	1118	1327	1103	1099	1023	1004	1075	1227
Discharge Frequency, f (Hz)	0.658	0.657	0.655	0.654	0.657	0.658	0.655	0.670	0.670	0.681
Impulse Bit, I (μ lb-sec)	1576	1800	1705	2029	1680	1670	1562	1498	1605	1801
Mass per Discharge, m_d (μ lb)	1.812	2.303	2.097	3.275	2.274	1.999	1.717	1.535	1.878	2.148
Specific Impulse, I_{sp} (sec)	870	782	813	620	739	835	910	976	855	838
Thrust-to-Power, T/P (μ lb/watt)	5.55	6.04	5.75	6.88	5.54	5.53	5.32	5.31	5.32	5.84
Engine Efficiency, η (%)	10.53	10.30	10.19	9.30	8.93	10.07	10.55	11.29	9.91	10.67
Energy Transfer, Efficiency, η_E (%)	63.48	62.16	62.94	60.04	60.94	62.21	56.40	75.49	50.43	56.27
Initial Inductance, L_o (nh)	104.3	136.4	83.8	152.8	135.5	119.1	177.4	220.4	183.8	164.0
Initial Impedance, Z_o (milliohm)	39.33	44.98	35.25	47.61	44.83	42.03	51.30	57.18	57.22	49.32
Eroded Mass/Ablated Mass, m_e/m_d	.0186	.0185	.0284	.0089	.0469	.0224	.0516	.0359	.0460	-
Propellant Area, A_p (sq. in.)	9.29	7.49	8.16	8.51	10.27	13.22	4.70	5.29	4.31	5.98

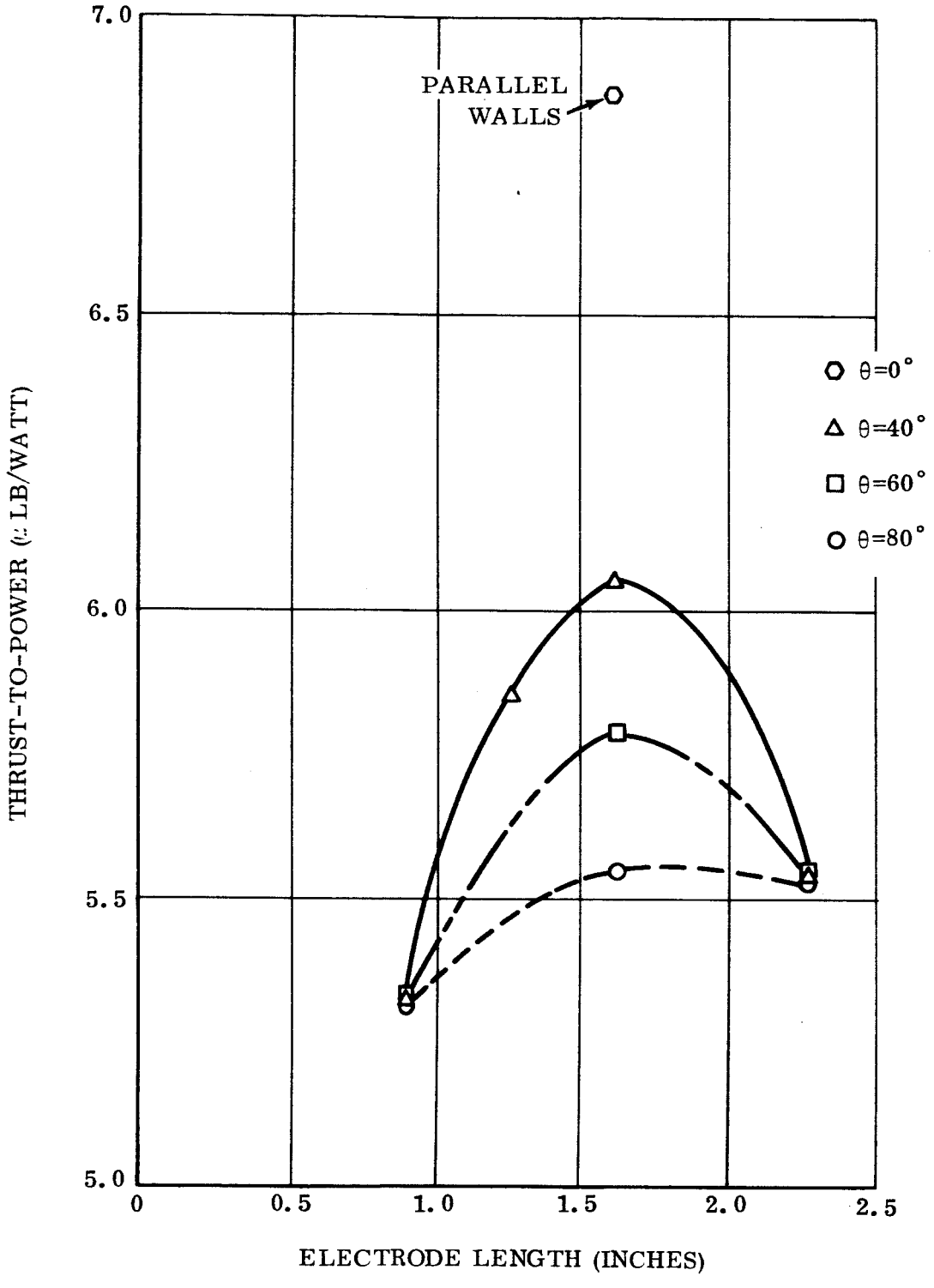

Figure 6. Thrust-to-Power as a Function of Electrode Length ℓ and Included Angle θ

observed as the included angle was decreased, it was reasoned that an angle of zero degrees (i.e., two flat sidewalls spaced a distance apart) should produce a higher thrust-to-power than any of the V-shaped propellants tested. Hence, an exploratory experiment utilizing a geometry consisting of 2 parallel propellant surfaces spaced 0.4" apart and having a 60° diverging flare at the exit plane was tried (see Figure 7). This configuration produced a thrust-to-power of 6.88 μ lb/watt (145 watts/m lb), verifying the hypothesis that the thrust/power ratio could be increased by decreasing the included angle. When one considers this result it

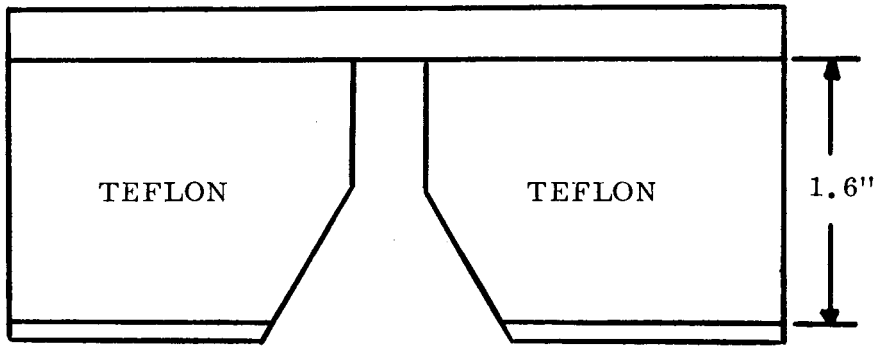

Figure 7. Cross-section of Parallel Side Wall Propellant Geometry

becomes obvious that the breech-fed geometry, with T/P typically 4 μ lb/watt, is just the special case $\theta = 180°$ of the side-fed geometry. Conceivably, therefore, one might postulate that converging propellant walls (θ negative) would produce even larger thrust-to-power ratios and wedge shaped propellant ($\theta > 180°$) a lower thrust-to-power ratio. A check of this hypothesis was beyond the scope of the present effort.

4.2 SPECIFIC IMPULSE AS A FUNCTION OF GEOMETRY

The variation in specific impulse with electrode length and included angle is presented in Figure 8 where a previously known correlation between specific impulse and initial energy per unit propellant area is plotted. Included in this figure are representative data for the breech-fed geometry. Again it appears that the breech-fed geometry is the special case of $\theta = 180°$. Roughly, as the included angle of the V-shaped propellant decreases at any given value of initial discharge energy and electrode length, specific impulse decreases even though the energy to area ratio will increase as a result of the decrease in included angle. Fortunately, the decrease in specific impulse is compensated for by an increase in the thrust/power ratio so the efficiency remains about the same. The conclusion to be drawn from the specific impulse data is that the slope of the lines of specific impulse (I_s) as a function of discharge energy/propellant area ratio presented on log-log paper decreases as the thrust-to-power ratio increases. Thus, even though the conclusion drawn from the original correlation (namely, that specific impulse increases monotonically with the energy/area ratio) is still valid, a larger increase in the energy/area ratio is required at higher values of thrust/power ratio to produce the corresponding increase in specific impulse achieved at lower thrust/power ratios.

4.3 PRODUCT OF IMPULSE x SPECIFIC IMPULSE AS A FUNCTION OF DISCHARGE ENERGY

One additional previously known correlation (Reference 1) is a plot of the product of impulse bit amplitude with specific impulse ($I \times I_s$) as a function of initial energy. Figure 9 presents the correlation including data of this study. Also indicated on this plot are lines of constant thrust efficiency derived from the general definition of efficiency rewritten as:

$$I I_s = .459 \times 10^5 \eta E_o$$

with E_o expressed in joules and $I I_s$ in μ lb-sec^2. As evidenced by this plot an increase in the initial stored energy will result in an increase in efficiency, all other parameters remaining constant. This correlation has been verified analytically during this experimental effort. Details of the analysis are presented in Appendix A of this report.

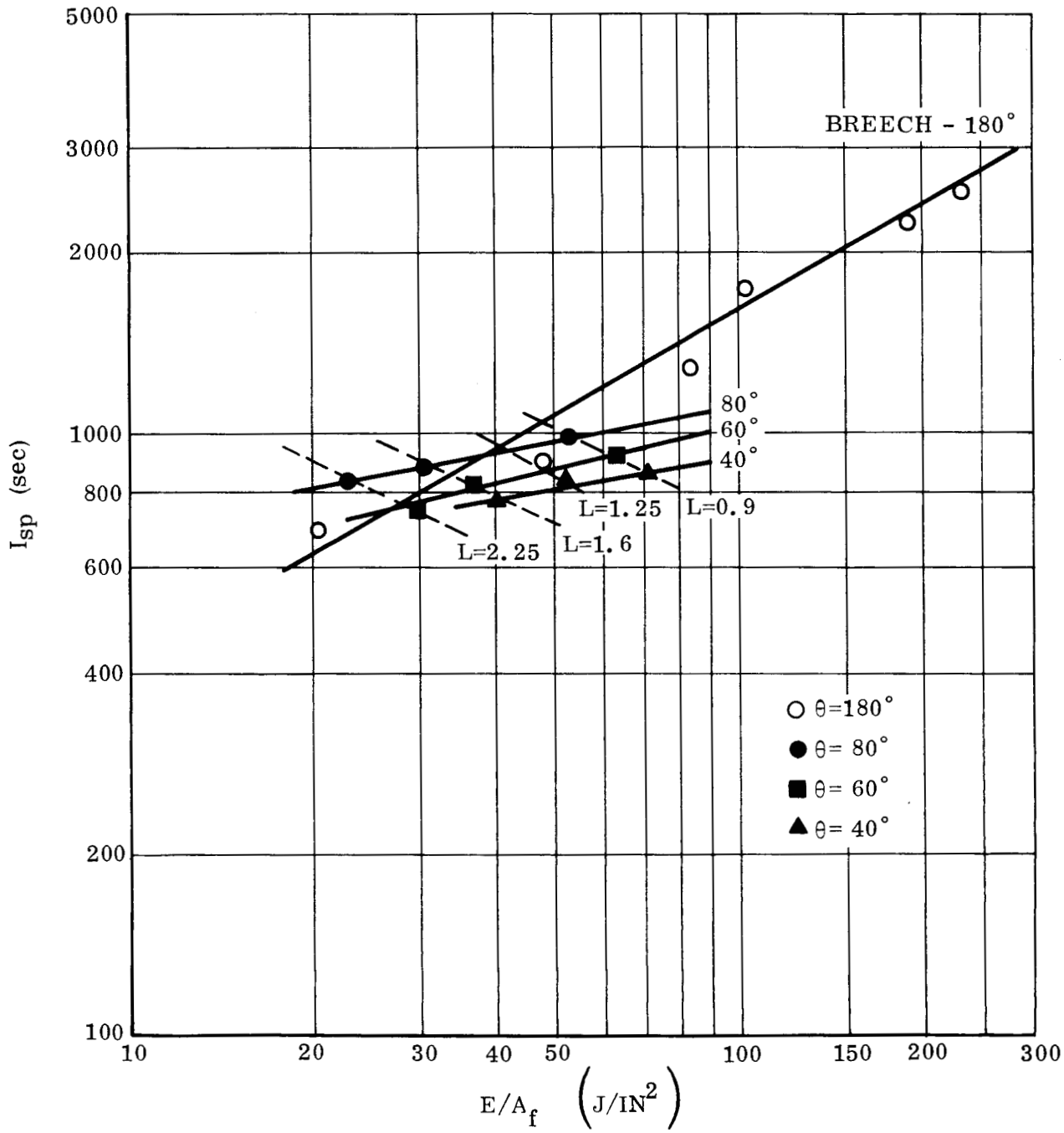

Figure 8. Specific Impulse as a Function of Initial Energy to Propellant Area Ratio

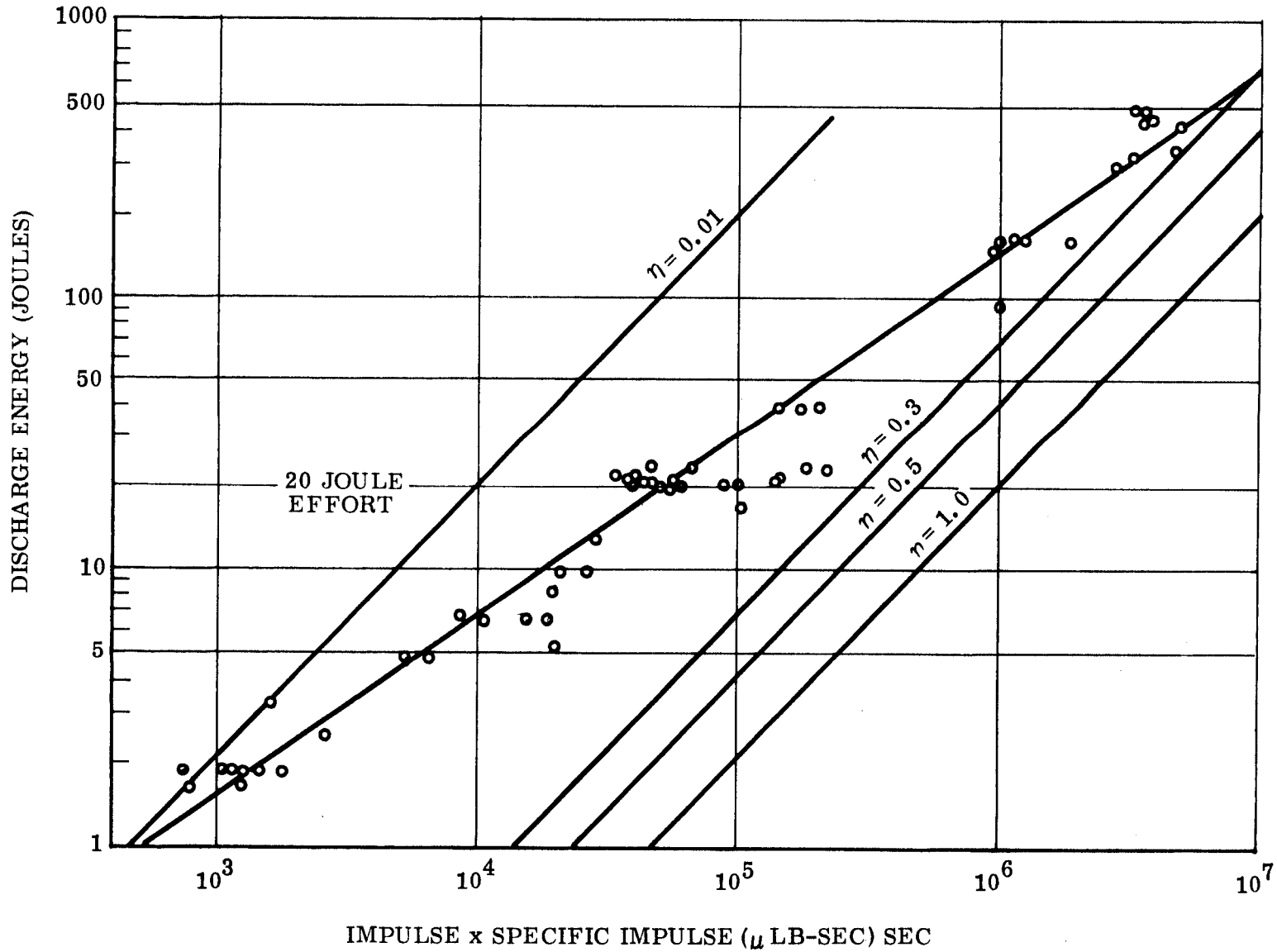

Figure 9. Product of Impulse Bit and Specific Impulse as a Function of Initial Energy

The increase of efficiency with discharge energy was twice demonstrated during the present program when two 500 joule tests were performed. The results of these two tests are presented in Table 2. In the first test (log 135-17) the parallel propellant side wall geometry was used with ℓ = 1.60 in. The thrust-to-power increased slightly from 6.88 (log 135-7) to 7.08μ lb/watt while the specific impulse showed an increase from 620 sec to 873 sec resulting in an increase in efficiency from 9.3% at 295 joules to 13.5% at 521 joules. The second 500 joule test (log 135-18) was performed using a 40° included angle and an electrode length of 1.25 in. Again, the thrust/power ratio increased from 5.84 (log 135-19) to 6.67 μ lb/watt and the specific impulse from 838 sec to 1119 sec leading to an increase in efficiency from 10.7% at 308 joules to 16.3% at 520 joules.

Prior to performing the two 500 joule tests it was believed that the thrust/power ratio of a given propellant-electrode configuration was virtually independent of discharge energy. The results of experimental studies on the breech-fed thruster seemed to indicate that this was the case since over the range of discharge energies from 2 joules to 300 joules the thrust/power ratio remained essentially constant around 4μ lb/watt. The increase in efficiency as discharge energy was increased for a given geometry was attributed to the expected increase in specific impulse resulting because an increase in discharge energy produced a corresponding increase in the energy to propellant area ratio. It is now observed that for the propellant side-fed configuration an increase in discharge energy also leads to an increase in the thrust/power ratio.

4.4 THRUST/POWER RATIO AS A FUNCTION OF PROPELLANT MASS

A critical examination of the experimental data revealed that an increase in discharge energy also causes an increase in the amount of ablated propellant mass per discharge. It was also noted from all available data that a trend existed between increasing thrust/power ratio and propellant mass (m_d). A plot of the thrust/power ratio as a function of mass per discharge (m_d) on log-log paper (See Figure 10) indicates that a rather general correlation does exist between the two, although scatter is evident. The majority of the scatter appears in the region where the propellant mass m_d per discharge is on the order of 10^{-4} kg (0.1 μ lb). The data represents discharge energies ranging from 1.5 to 520 joules and also includes several different thruster geometries previously

TABLE 2. RESULTS OF 500 JOULE PERFORMANCE TESTS ON SIDE-FED CONFIGURATIONS

Log No.	135-17	135-18
ℓ (inches)	1.6	1.25
θ (degrees)	0	40
N	3260	3042
C (μ fd)	114.5	114.5
V_o (KV)	3.02	3.01
E_o (Joules)	521	520
T (μ lb)	2511	2020
f(Hz)	0.681	0.583
I (μ lb-sec)	3687	3467
m_d (μ lb)	4.226	3.099
I_{sp} (sec)	873	1119
T/P (μ lb-watt)	7.09	6.67
η (%)	13.47	16.27
η_E (%)	51.62	59.80
L_o (nh)	111.9	132.7
Z_o (milliohm)	31.26	34.04
m_e/m_d	.0272	.0752
A_p (sq. in)	8.51	5.98

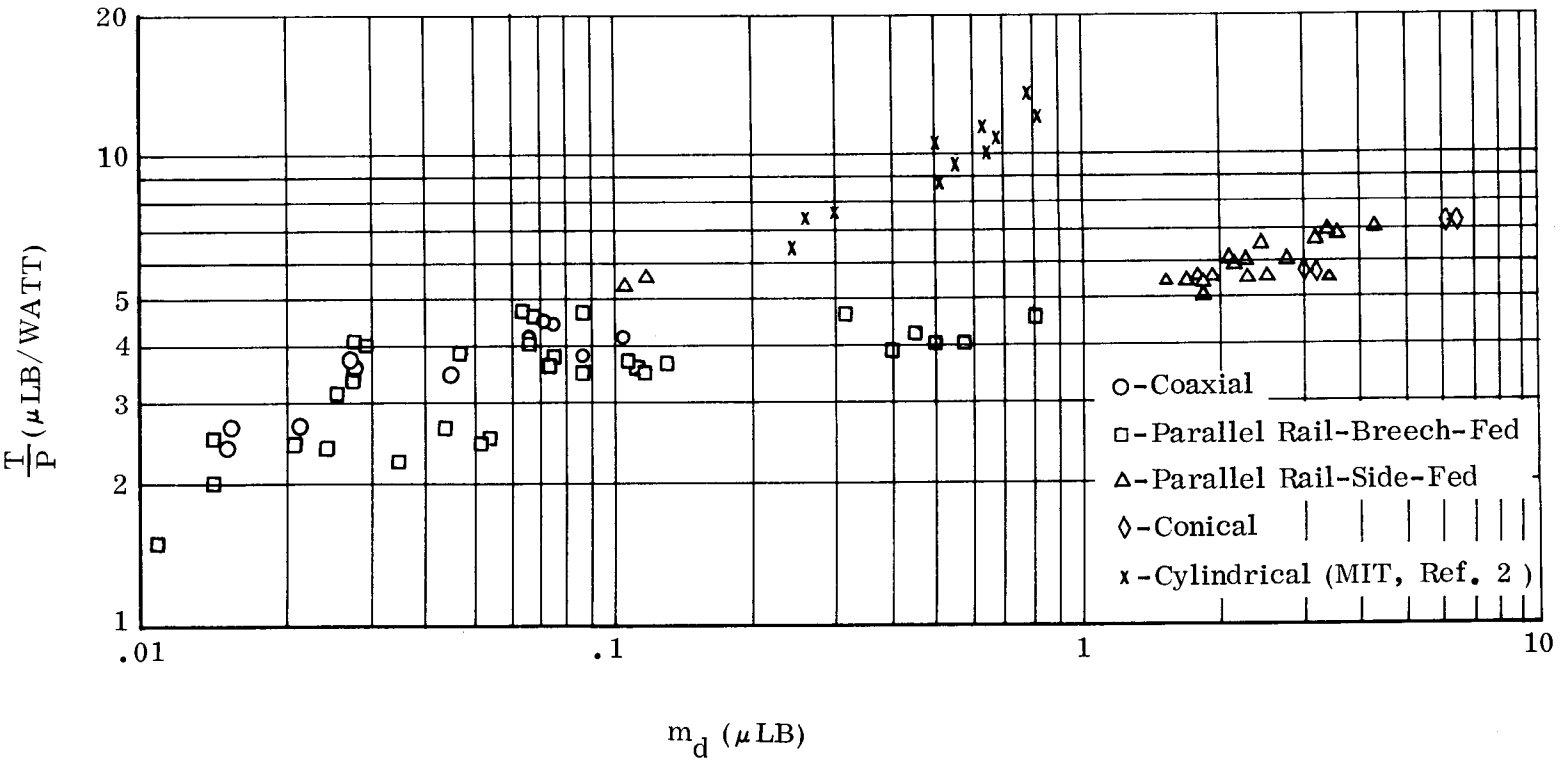

Figure 10. Thrust-to-Power as a Function of Ablated Mass per Discharge

tested at Republic as well as the data obtained during this program. Also included are data obtained through the courtesy of the MIT Aeronautics Department[2] on a cylindrical solid teflon propellant geometry. The initial energy used by MIT is 20 joules. These results, coupled with our own, suggest the presence of distinct trend lines superposed upon the rather general correlation of T/P versus m_d. These superposed trend lines exhibit both an energy dependence and a dependence upon the geometry of the thruster. Generally speaking, it appears that if initial energy is maintained constant and geometry is changed so as to produce more mass per discharge, the thrust/power ratio will increase along one trend line. If, on the other hand, the geometry is fixed and energy is increased to increase m_d, thrust-to-power will increase along a different trend line. The observation that m_d is indeed both geometry and energy dependent will be further supported by the results to be presented in Section V.

A dependence of thrust/power on propellant mass per discharge is suggested from results of idealized gasdynamic considerations. If a fixed mass (m) of quiescent gas having an energy E is suddenly allowed to escape into vacuum the maximum obtainable impulse bit would be given by

$$I_{GD} = F(\gamma)\,(2mE)^{1/2} \tag{1}$$

where γ is the ratio of specific heat at constant pressure to specific heat at constant volume. From this expression one obtains

$$\left(\frac{T}{P}\right)_{GD} = \left(\frac{I}{E}\right)_{GD} = F(\gamma)\left(\frac{2m}{E}\right)^{1/2} \tag{2}$$

$$I_{s_{GD}} = \left(\frac{I}{m}\right)_{GD} = F(\gamma)\left(\frac{2E}{m}\right)^{1/2} \tag{3}$$

and

$$\eta_{GD} = F(\gamma) \tag{4}$$

According to these idealized considerations, the gasdynamic contribution to the impulse bit is directly proportional to the square root of the mass per unit energy. At fixed energy this would imply $(T/P)_{GD} \propto m^{1/2}$. If one considers m to be the mass per discharge m_d and E the initial stored energy E_o the

observed increase in T/P with m_d at constant energy would agree with the above idealized considerations. Hence, at first glance it would appear that the observed increase in T/P with m_d is primarily a gasdynamic effect.

Since in Section V of this report, it will be shown that the propellant mass correlates with the integral $\int i^2 dt$ and a geometric factor, the observed increase in thrust/power ratio could also be electromagnetic in origin. This conclusion is based upon the observation that an increase in the magnitude of the integral $\int i^2 dt$ simultaneously increases both the propellant mass (i.e., gasdynamic contribution to the thrust) and the magnetic pressure force.

Generally both magnetic and gasdynamic processes must be considered in plasma acceleration unless it can definitely be proven that one of these processes has a very small effect on the velocity, in comparison to the other.

4.5 RESULTS OF EXPLORATORY EXPERIMENTS ON A CONICAL PROPELLANT CONFIGURATION

At the onset of this program some exploratory experiments on a conical fuel geometry having rectangular cross-section were performed. Two different geometries were tested; one with zero degree included angle and the other having a 40° included angle. All tests were performed at 300 joules. A photograph of the assembly mounted on the thrust balance is included in Figure 11. The cathode and igniter plug were located at the upstream apex end of the cone whereas the anode was positioned at the downstream end. The downstream opening (exhaust area) in the anode was slightly smaller than the downstream opening in the conically shaped teflon propellant. The small anode lip that extended beyond the teflon propellant into the interior of the cone served as an exposed electrode to the axially directed arc discharge. Results of these exploratory tests involving conical shaped propellants, are presented in Table 3. The conclusions to be drawn from these results are much the same as those obtained from the data on the side-fed thruster; namely, that an increase in the included angle decreases the thrust/power ratio. Thrust/power dependence upon propellant mass for the conical configuration also follows the same general trend as the data on all other geometries.

TABLE 3. RESULTS OF EXPLORATORY 300 JOULE TESTS ON CONICAL CONFIGURATIONS

Log	134-2	134-5
ℓ (in.)	1.6	1.6
θ (degrees)	0	40
N	3115	2743
C (μ fd)	67.4	67.4
V_o (KV)	2.93	2.81
E_o (Joules)	289	266
T (μ lb)	1433	435
f (Hz)	0.677	0.286
I (μ lb-sec)	2118	1522
m_d (μ lb)	6.089	2.965
I_s (sec)	348	513
T/P (μ lb/watt)	7.34	5.72
η (%)	5.57	6.40
A_p (sq. in.)	9.70	10.50

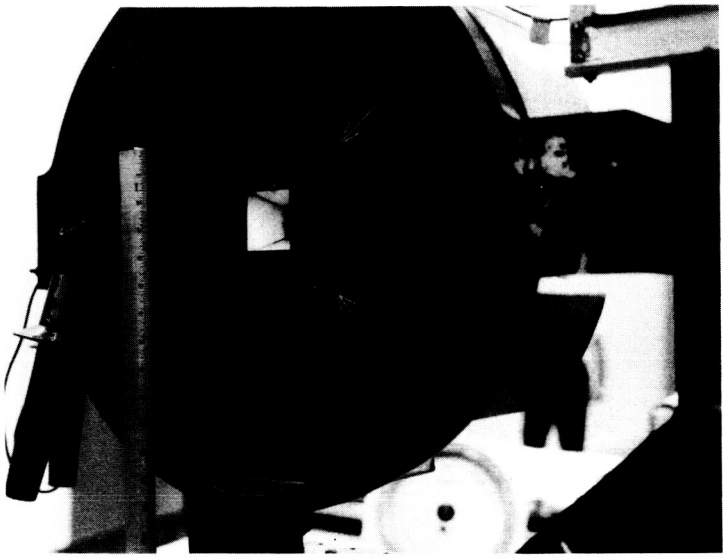

Figure 11. Conical Engine Mounted on Thrust Balance

4.6 COMPARISON WITH GASEOUS PROPELLANT PULSED PLASMA THRUSTER

One of the main results of this study is the conclusion that the impulse/energy, i.e., thrust/power ratio of the solid propellant pulsed plasma thruster is a function of propellant mass per discharge, with several additional trend lines (apparently due to geometry) superposed on the general correlation. The only known study of a gaseous propellant pulsed plasma thruster encompassing large changes in the thrust/power ratio is reported in Reference 3. In that study a given switch triggered pulsed plasma thruster geometry was located on a thrust balance in a vacuum chamber and operated at a fixed discharge energy. The vacuum chamber background pressure, and thus the interelectrode pressure, was varied from about 30 microns to about 10,000 microns and thrust behavior was determined as a function of the uniform initial pressure. Since the interelectrode volume was fixed, the mass of gaseous propellant in the interelectrode spacing is directly proportional to the initial pressure. Figure 12 presents thrust/power as a function of interelectrode pressure (i.e., proportional to propellant mass) as reported in Reference 3. It is interesting to note that both the gaseous propellant and solid propellant results show an increase in

thrust/power with an increase in propellant mass per discharge. The presence of several data trend lines making up the general correlation between thrust/power and pressure (i.e., mass) was also observed in Reference 3. A similarity thus exists between the thrust/power variation with propellant mass for both the solid propellant and the gaseous propellant pulsed plasma thruster. Since insufficient data is presented in the literature, it was not possible to ascertain if the general correlation between thrust/power ratio and propellant mass applies quite generally to pulsed plasma thrusters independent of type of propellant, geometry and discharge energy level.

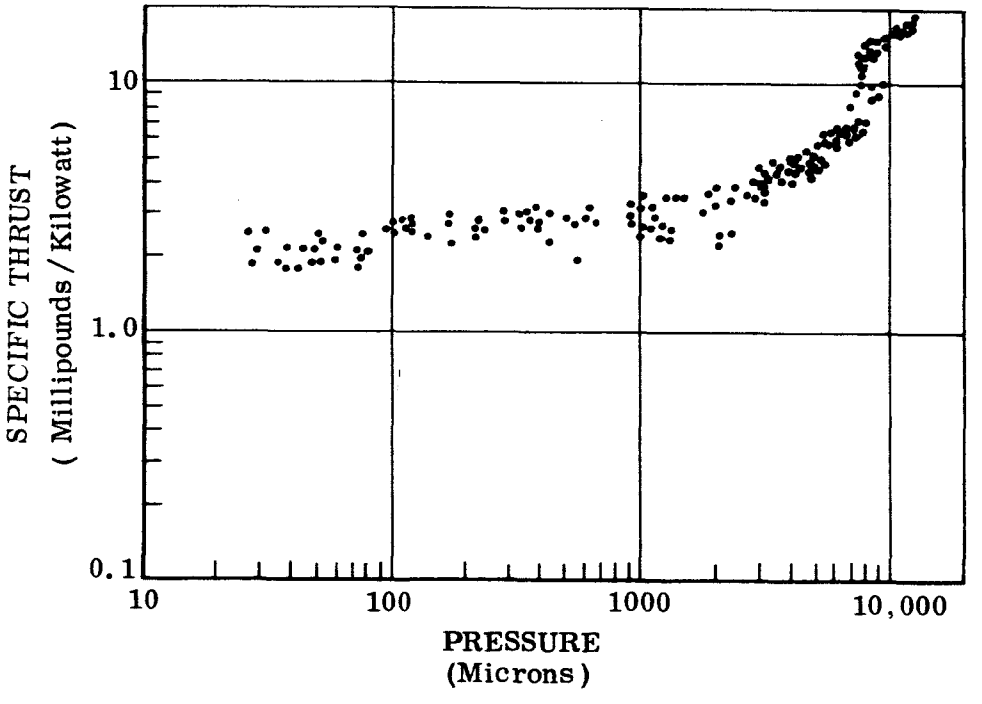

Figure 12. Thrust-to-Power as a Function of Interelectrode Propellant Pressure for Gaseous Propellant Thruster

SECTION V

PROPELLANT ABLATION STUDY

Since the mass per discharge has been shown to be the parameter of primary interest regarding the magnitude of thrust-to-power it is essential that a relationship between propellant mass and controllable engineering parameters be found.

A brief examination of the literature on ablation has yielded a useful result. To first order, the rate of mass ablation from a thermal insulator is proportional to the flux of energy per unit time per unit area impinging on the surface. If it is assumed that the energy absorbed by the plasma through resistive heating is converted to some degree into radiant energy, then the radiant energy per unit time emitted by the plasma will be proportional to the current (i) squared. The percentage of this radiant energy flux impinging on the propellant surface will be given roughly as the ratio of propellant area to open area existing at the boundaries of the plasma before it leaves the exit plane of the electrodes. Hence,

$$\dot{m} \propto \frac{A_p}{A_o} i^2 \tag{5}$$

where A_o is the open area of the plasma boundaries. Hence,

$$m_d = \int_o^\infty \dot{m} dt \propto \frac{A_p}{A_o} \int_o^\infty i^2 \, dt \tag{6}$$

For the V-shaped geometry the ratio A_p/A_o is equal to the cosecant of the half angle between propellant walls. For the breech-fed geometry, the factor A_p/A_o is difficult to estimate since the plasma will expand laterally beyond the electrode surfaces as mass ablates. With no knowledge of the expansion angle, evaluation of A_o is not possible. Figure 13 is a plot of results using this simplified relationship.

Some data was available from earlier tests on the breech-fed geometry in which Mykroy side-walls were located on the downsteam sides of the electrodes. In such a case $A_p/A_o = 1$ and that data could be used in the correlation. Since those tests were done at lower energies (5 and 10 joules) the data allowed us to

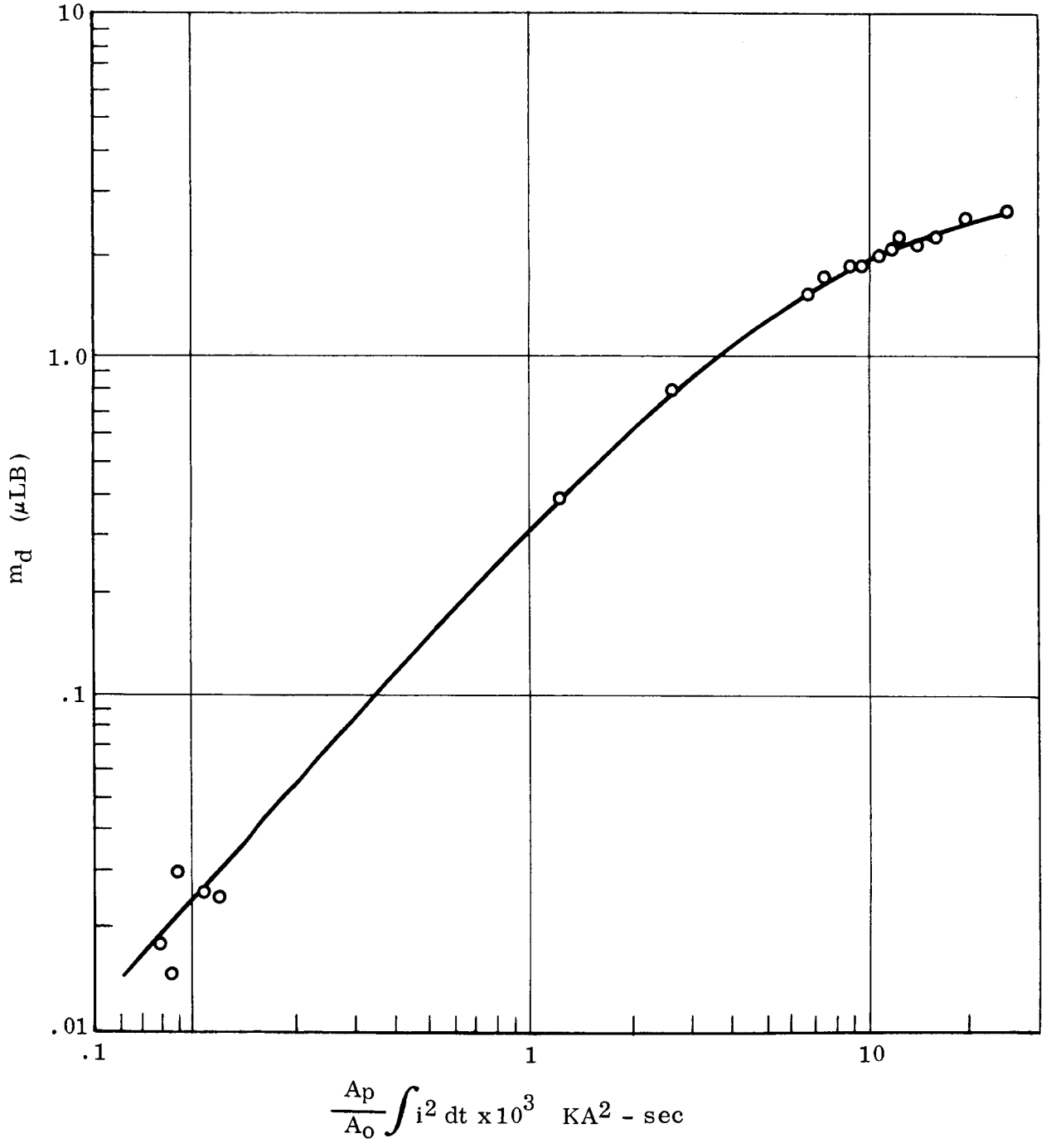

Figure 13. Ablated Mass per Discharge as a Function of $(A_p/A_p)\int i^2\,dt$

verify the above correlation two orders of magnitude lower than the data generated in the present program. No complete set of data exists for the intermediate order-of-magnitude regime so verification of the correlation in this region is not possible at this time. It is interesting to note that when the mykroy side-walls were removed and the identical thruster retested, an increase in specific impulse and decrease in thrust/power was observed. Based on the previous argument this can now be understood since by removing the walls the radiant energy in the plasma was no longer confined and less mass was produced thereby increasing the specific impulse while decreasing the thrust/power ratio.

Unfortunately, the integral $\int i^2 dt$ is not a useful parameter from an engineering point of view since it is not known how to design a circuit (which includes the thruster) to produce specific values of this parameter. Evaluation of the integral $\int i^2 dt$ for an LRC circuit with fixed elements reveals that:

$$\int_0^\infty i^2 \, dt = \frac{E_o}{R} \qquad \text{(Fixed LRC)} \tag{7}$$

where R is the resistance. For a thruster the resistance of the circuit plus the arc is generaliy apriori unknown so the above result is of no help from an engineering standpoint except to indicate that an increase in E_o will cause an increase in the magnitude of the integral $\int i^2 dt$. An alternate way to find out what parameters will change the magnitude of this integral is to nondimensionalize i and t with respect to characteristic values. Noting that $i = C\,(dV/dt)$ we may nondimensionalize V with respect to V_o and t with respect to $\sqrt{L_o C}$ and find the characteristic current to be $V_o(C/L)^{1/2}$. Substitution of $i = \bar{i}\, V_o\, (C/L)^{1/2}$ and $t = \bar{t}\ \sqrt{L_o C}$ yields:

$$\int_0^\infty i^2 \, dt = \frac{C V_o^{\,2}}{\sqrt{L_o/C}} \int_0^\infty \bar{i}^{\,2} \, d\bar{t} \tag{8}$$

Thus, the integral $\int i^2 dt$ in its dimensional form should follow the same trend in order-of-magnitude as the energy divided by the initial impedance $Z_o = (L_o/C)^{1/2}$. This hypothesis is verified by the data presented in Figure 14 where the integral $\int i^2 dt$ is plotted as a function of the initial energy to impedance ratio. The initial inductance used in computing Z_o is given by $L_o = V_o (di/dt)^{-1}$.

This correlation is extremely useful since it has enabled us to examine our conclusions concerning the ablation of mass with the results of experimental work done in Russia[4] on short pulse discharge ablation. The cited research was performed with a conical accelerator geometry and was directed at determining what parameters influence the amount of ablated mass per discharge (m_d). Inductance, capacitance and stored energy were varied independently in the Russian study and the conclusions reached were:

a) As stored energy increases so does mass per discharge
b) As initial inductance increases mass per discharge decreases
c) As capacitance increases so does mass per discharge.

Our conclusions are identical to those since the correlation in Figures 13 and 14 lead to the analytical expression:

$$m_d \propto \frac{A_p}{A_o} \frac{E_o}{Z_o} = \frac{A_p}{A_o} \frac{E_o}{(L_o/C)^{\frac{1}{2}}} \propto \frac{A_p}{A_o} \int i^2 \, dt \qquad (9)$$

Hence, Equation (9) encompasses all of the conclusions of Reference 4 and is more comprehensive since it includes the electrical characteristics in one parameter and also includes the appropriate geometric factor.

Increasing the geometric factor A_p/A_o will increase m_d. This factor has a strong effect on ablated propellant mass as demonstrated by the data obtained during this study in which the integral $\int i^2 dt$ varied only between about 3.3 and 6.7 x 10^{-3} KA^2 sec whereas A_p/A_o varied between 0.2 and 5.0. Indeed there were some cases in which the integral was smaller than in others and yet the ablated propellant mass was larger since the geometric factor A_p/A_o became the governing factor.

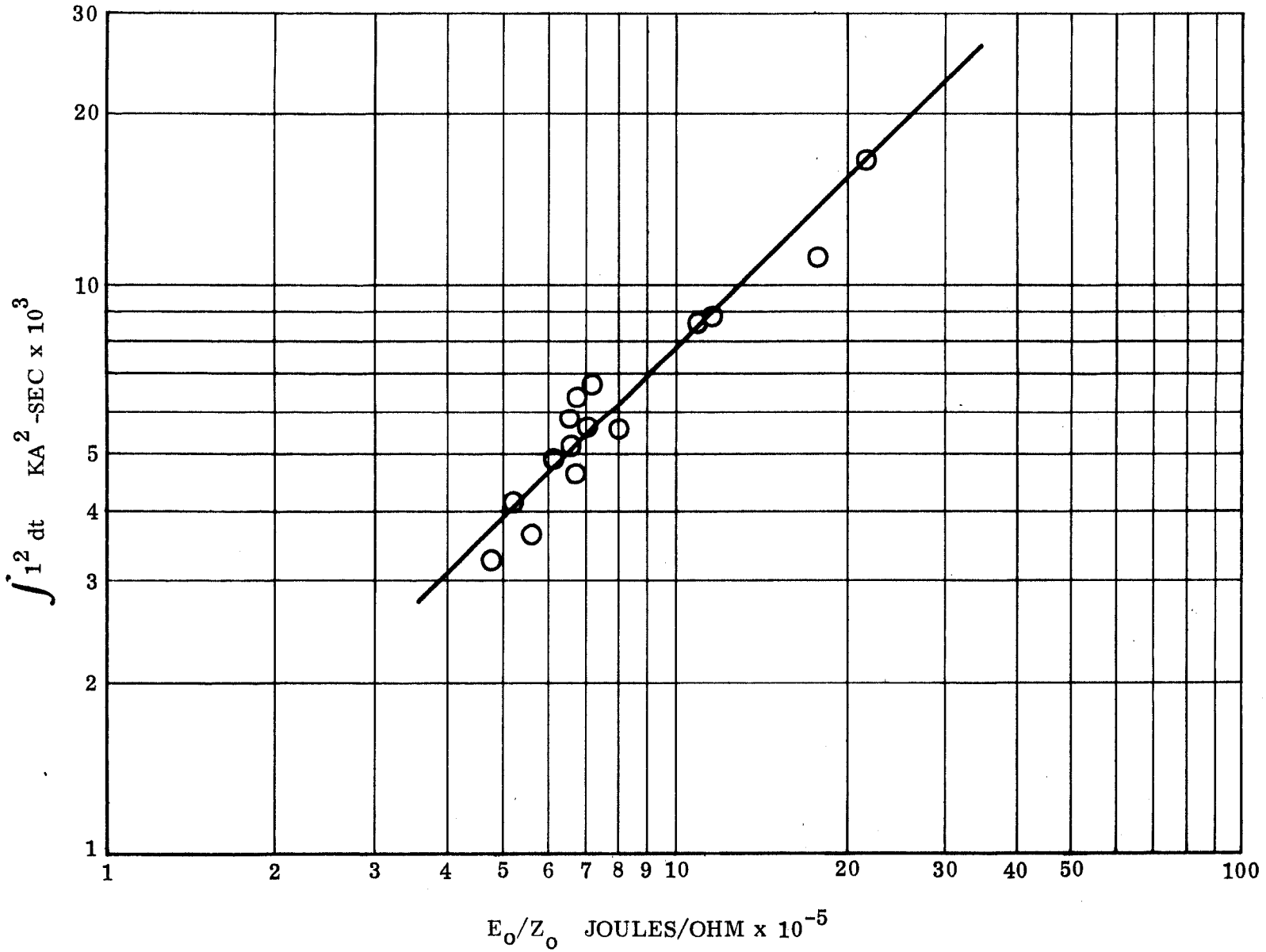

Figure 14. Integral of Current Squared as a Function of Initial Energy to Initial Impedance Ratio

SECTION VI

PRACTICAL ASPECTS OF A V-SHAPED PROPELLANT

The program being reported upon was primarily concerned with a study and understanding of the effect of propellant side-feed configurations on the magnitude of of the thrust/power ratio. V-shaped solid propellant configurations were used to implement the scheme of side feeding the propellant into the discharge. The results presented in this report have shown that such a propellant feed-scheme can significantly increase the magnitude of the thrust/power ratio over previously studied breech-fed configurations.

The question of how such a V-shaped propellant feed scheme could be practically implemented was briefly examined independently of the main effort of this program. The success of using a small feed retaining shoulder and propellant feed spring as the propellant feed system has been adequately demonstrated in the laboratory as well as in space for breech fed geometries. A low discharge energy (about 8.4 joules/discharge) microthruster was modified to supply a teflon rod from the breech end of the thruster into the accelerator nozzle. The end face of the teflon in the accelerator nozzle was machined to have a V-shaped cutout with an included angle of 90°. A correspondingly V-shaped fuel retaining shoulder was machined into the anode. A Negator spring assured, as in normal breech-fed configurations, that the propellant was always maintained against the anode shoulder. The complete thruster was mounted on a thrust balance and operated uninterrupted for a period corresponding to the delivery of the total impulse requirements of typical microthrusters in present spacecraft.

Figure 15 shows the thruster and the V-shaped propellant rod remaining after operating for 1440 hours at a pulse rate of 1.84 Hz.

The results of this test are tabulated below:

Performance of a V-Shaped Propellant Thruster (Log-129-3)

Continuous Thrusting Time	1440 hours
Test Average Thrust Level	74.2 μ lb
Test Average Impulse Bit	40.2 μ lb-sec
Total Length of Propellant Consumed	12.88 in.
Total Number of Discharges	9,590,163

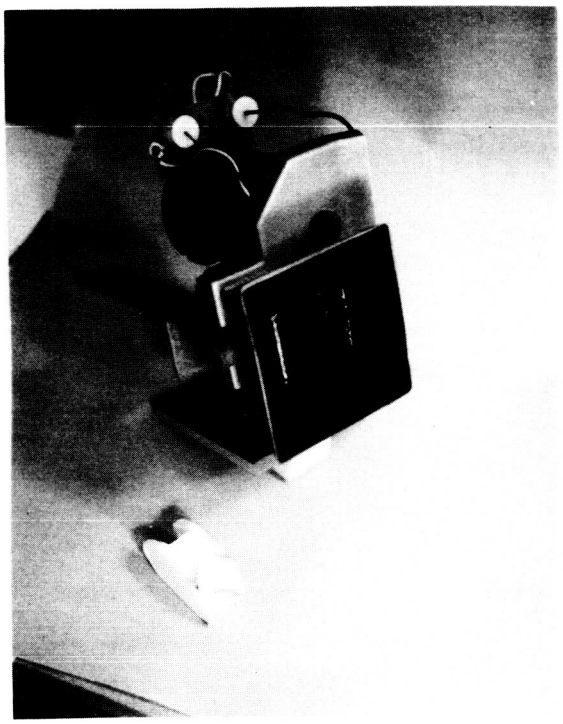

Figure 15. Endurance Tested Microthruster with V-Shaped Propellant

The data presented in the previous table are comparable to typical breech-fed microthruster data in terms of performance capability. This exploratory test has demonstrated the practicality of using a breech end supplied V-shaped propellant configuration in a pulsed plasma thruster. It is believed that feeding the V-shaped propellant from the sides instead of the breech end can also be easily implemented.

SECTION VII

ELECTRODE EROSION

All data on electrode erosion was taken as explained in Section III. In Reference 5 it was stated that electrode erosion in quasi-steady plasma devices is dependent upon the parameter $i^2/\dot{m}$. For solid propellant short pulse discharge thrusters it was found[1] that the counterpart of this parameter is $\int i^2 dt/m_d$. In the latter short pulse discharge thruster study, a correlation was found to exist between the amount of electrode erosion and the above stated parameter. The results of that study as well as the data obtained during this program are presented in Figure 16 where eroded mass m_e is plotted as a function of the parameter $\int i^2 dt/m_d$. The integral of current squared was evaluated numerically from oscilloscope traces of the discharge current. In all tests done in Reference 1 a tungsten anode and a stainless steel cathode were used in conjunction with a propellant breech-fed geometry. The thruster was usually fired for 9000 or more consecutive discharges

The reason that the trend lines depicted in Figure 16 are not coincident may be a result of the difference in anode material. This is conceivable since the anode will generally exhibit up to ten times as much erosion as the cathode. Another possibility for the difference is because the amount of erosion per discharge will decrease as the number of consecutive discharges increases. This observation is due to the initial high degree of erosion on sharp corners which gradually decreases as the corners become rounded. Thus, no firm conclusions can be drawn by comparing the two sets of data, but in both cases a definite trend toward increased erosion is evidenced as the parameter $\int i^2 dt/m_d$ is increased.

In the light of the excellent conductivity of copper, an attempt was made during this study to use copper as an electrode material. The configuration of a previously performed test was used and a copper anode replaced the original stainless steel anode. Less than one-tenth the anode erosion was evidenced when copper was used. Thus, in addition to being a much better electrical conductor, copper seems to erode to a lesser degree than stainless steel. Interestingly, the Russians have been using copper for electrodes at much higher energies than those being reported here.

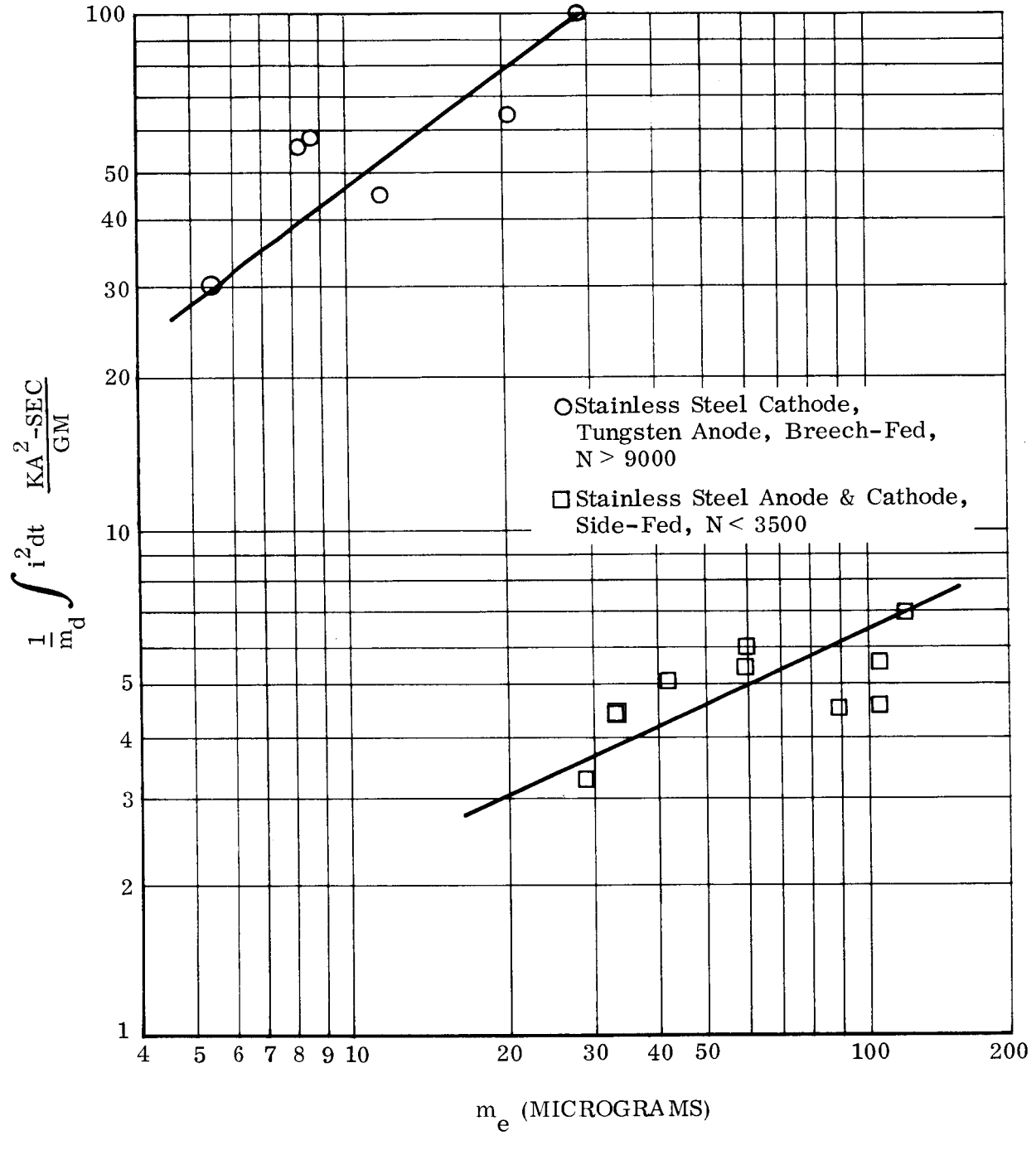

Figure 16. Eroded Electrode Mass per Discharge m_e as a Function of $\int i^2\,dt/m_d$

SECTION VIII

CAPACITOR LIFE TESTS

During the course of this effort two dry (no liquid impregnants) energy storage capacitors were purchased from Capacitor Specialists, Inc. (CSI).* Input specifications for the design of these capacitors were supplied using previous voltage and current data to predict discharge duration, percent voltage reversal and maximum expected current at the 300 joule energy level. Other primary design criteria were based on typical mission requirements; i. e., maximum operating temperature, high specific energy and high capacitor quality.

The first capacitor measured a capacitance of 63 μfd and was rated at 3 KV. The capacitor was rectangular in shape, measuring .178 m x .203 m x .229 m (.7" x 8" x 9") and weighing approximately 13.6 kg (30 lbs). The specific energy was therefore 4.55j/kg (10 j/lb) at 3.1 KV. The dielectric material used in construction was Kapton.

Electrical characteristics of the capacitor were evaluated by charging the capacitor using a 10 VDC source and discharging it in a minimum inductance shorted configuration through a thin strip of oxygen-free copper around which a Rogowski coil was placed. Current and voltage were recorded on an oscilloscope and from the current trace the inductance and resistance were computed. Details of that calculation are included in Appendix B of this report. The results of this test are summarized in Table 4 along with our specification for comparison.

TABLE 4. Comparison of Actual with Specified Capacitor Data

PARAMETER	SPECIFIED	COMPUTED
Inductance (nH)	≤ 7.0	24.93
Impedance (milliohm)	≤10.0	4.0
Resistance (milliohm)	≤ 1.0	3.62
Quality	≥10.0	5.74 (at .12 MC)

As indicated by the data, the capacitor supplied fell somewhat short of our requirements.

* Capacitor Specialists Incorporated, Del Dios Highway, Escondido, California

In addition to the above design criteria a maximum service temperature of 339°K (150°F), maximum current of 70,000 amperes, and maximum voltage reversal at 25% were specified. Design life was set at 20 million shots.

A photo of the first capacitor and engine components is included in Figure 17.

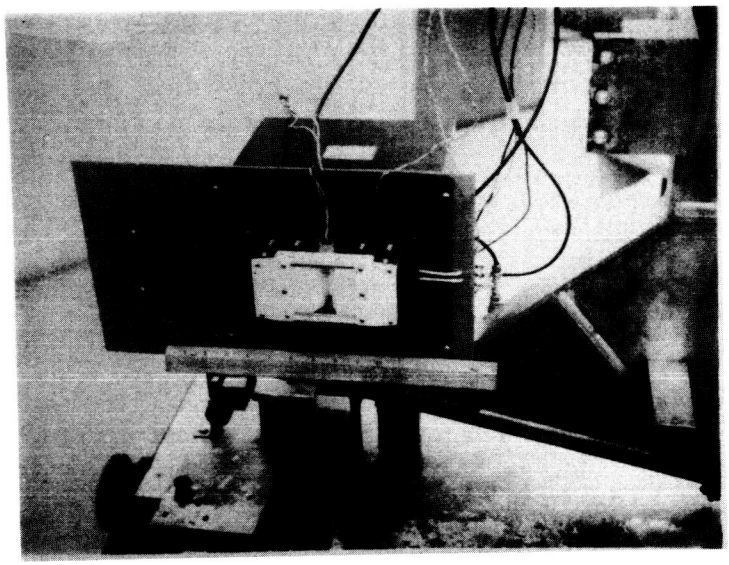

Figure 17. First CSI Capacitor and Engine Components Mounted on Thrust Balance

The first capacitor failed after delivering only 52 discharges. A 40 ohm resistance was measured across the strip lines and it was shipped back to the manufacturer for failure analysis. They concluded that failure occurred because of arcing between two of the end connection tabs. By isolating the shorted tabs they were able to repair the capacitor and have indicated that the capacitance of the repaired capacitor is now reduced to about 59 μfd. At the time of writing the repaired capacitor has not yet been received.

The second capacitor of the original two capacitors purchased delivered 4436 discharges before it also failed. A 2 ohm resistance was measured across its terminals and it also was sent back to the manufacturer for failure analysis. No word has been received as to the reason for failure at the time of this writing.

Unfortunately neither capacitor lasted long enough to perform a thruster performance test to permit a comparison of results with an identical electrode-

propellant geometry on the original 10 year old capacitor bank used during this study. It was found that our original very low inductance design approach, in which the electrodes were attached directly to the capacitor strip line terminals, was unacceptable due to thermal conditions. Thermocouples mounted on the face of the capacitor (between the capacitor terminals) and on the negative strip line itself indicated a steady rise in temperature during thruster operation. The temperature increased from room temperature to about 337° K (146°F) at the strip line in approximately 17 minutes. The thruster design was therefore modified by providing radiative surfaces between the electrodes and capacitor terminal strip lines so as to remove heat through radiation before it reached the capacitor. The modified design is shown in Figure 18.

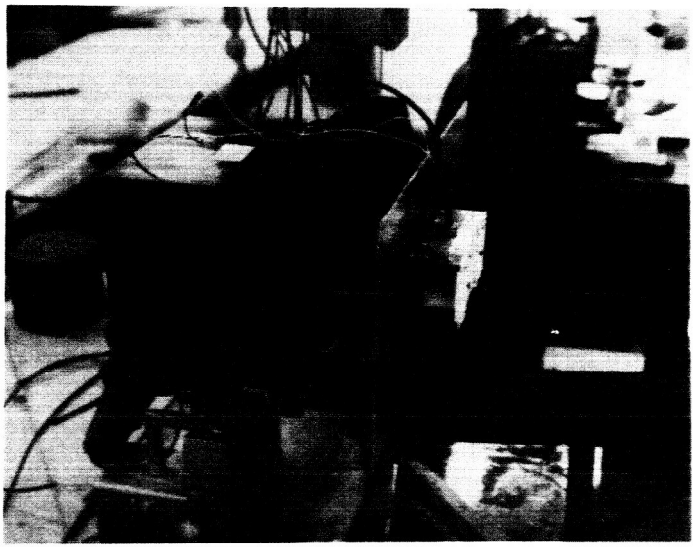

Figure 18. Second CSI Capacitor and Engine Components Mounted on Thrust Balance Showing Radiator Surfaces.

The radiators are 3.7 mm thick copper separated by 1.2 mm teflon sheet to provide a minimum inductance. The exterior surfaces are painted with a black epoxy base paint and sandblasted to optimize the surface emissivity. A plot of temperature vs time for both designs is presented in Figure 19. From the data it is obvious that the addition of radiators proves to be an efficient technique for cooling. The temperature was leveling off but the equilibrium state was never reached since the capacitor failed before the test was completed. The use of heat pipes for this purpose is another possibility to maintain minimum inductance.

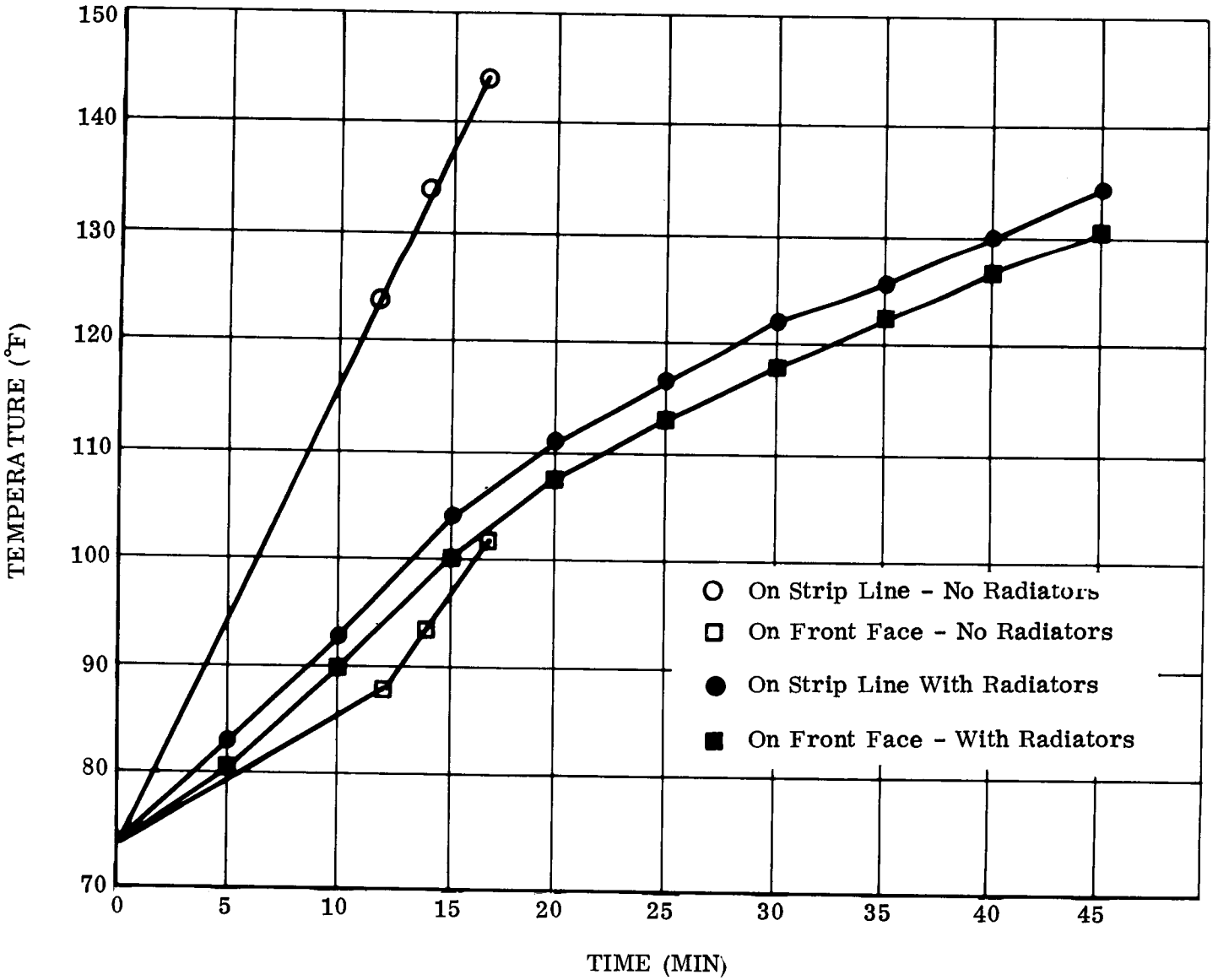

Figure 19. Temperature of Strip Line and Face of CSI Capacitor as a Function of Time.

The only performance parameter which could be evaluated during these tests was the energy transfer efficiency η_E. The data obtained with the CSI capacitor and copper electrodes yielded $\eta_E = 79.9\%$ while the original bank using stainless steel electrodes and the same electrode-propellant geometry produced $\eta_E = 60.0\%$. The initial overall inductance was calculated to be 152.8 nanohenries on the original thruster and 44.06 nanohenries on the thruster utilizing the CSI capacitor. Thus, the capacitor received from CSI delivered more energy at a much faster rate than the original capacitor bank. This fact is further illustrated in Figure 20 where the power per unit of initial energy is plotted as a function of time. It is observed that the major portion of the total energy delivered is supplied during the first half-cycle of the discharge. Maximum power is approximately 74% larger for the engine utilizing the CSI capacitor and the duration of the initial spike is almost 1.5 microseconds shorter.

Tentatively it would appear that the state-of-the-art of dry (no liquid impregnation) energy storage capacitors suitable for application to pulsed plasma thrusters has not advanced to the level of reliability of liquid impregnated units when compared on the same joules/lb basis.

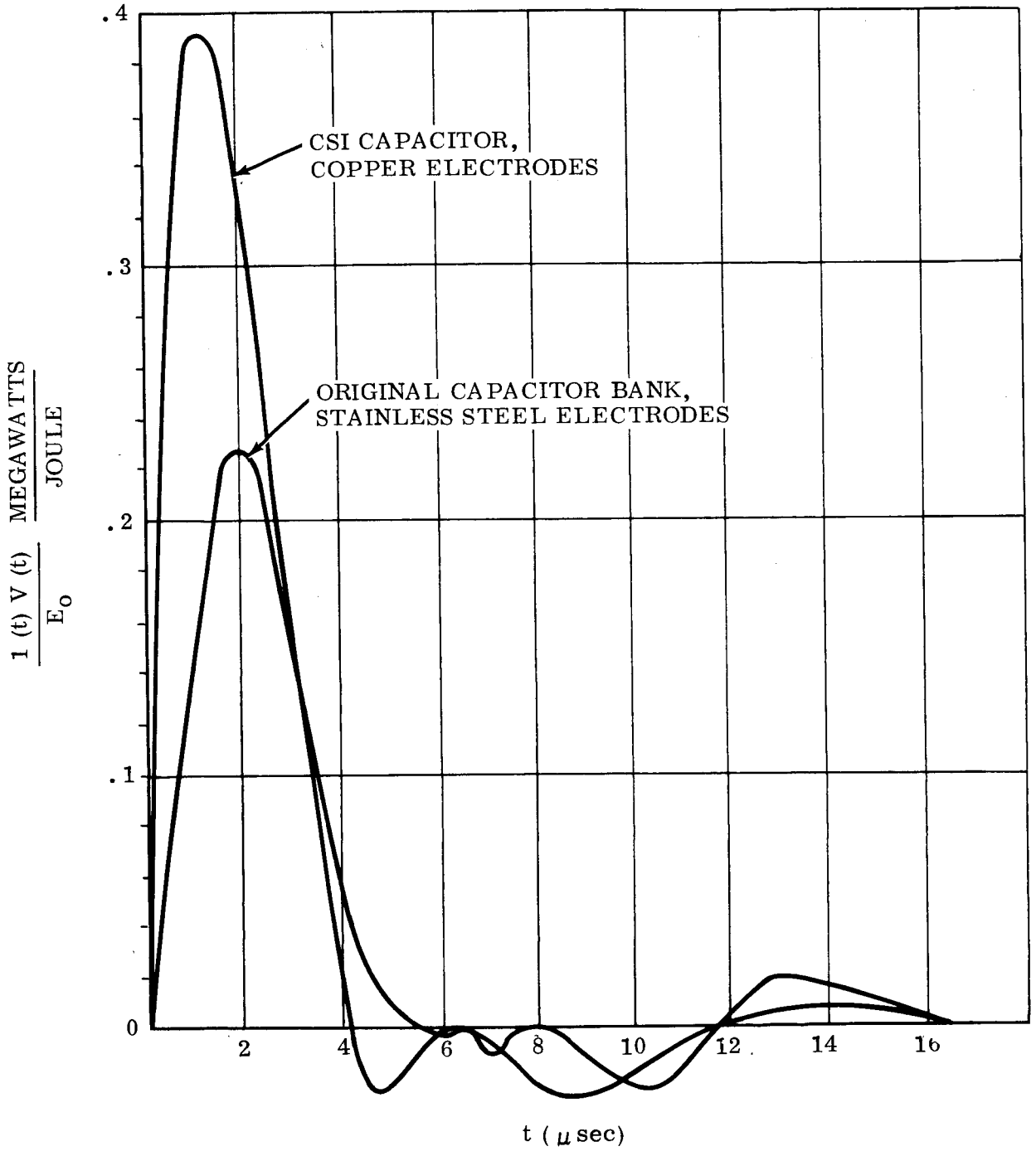

Figure 20. Power Per Unit of Initial Energy as a Function of Time for CSI Capacitor and Original Capacitor Test Bank

SECTION IX

CONCLUSIONS

This program was primarily concerned with an evaluation of the technique of feeding solid propellant into the discharge from the sides of the accelerator nozzle and to examine how this technique effects the thrust/power ratio. In particular, the effects of included angle of V-shaped propellants and of electrode length were examined. While these particular parameters effected the magnitude of the thrust/power ratio, and in some cases significantly, it was found that at a given value of initial energy it is the quantity of propellant mass which more generally correlates with the thrust/power ratio. While a similar result has been observed in a gaseous propellant pulsed plasma thruster, for the ablative thruster the geometric parameters become a specific means of governing the amount of mass produced per discharge.

Normally one might therefore deduce the observed thrust/power ratio behavior to be gasdynamic in origin. However, for the ablative thruster studied the mass per discharge was found to correlate with the integral $\int i^2\,dt$ and a geometric factor. Since the electromagnetic contribution to thrust also depends directly upon these latter parameters it is concluded that increasing the integral $\int i^2\,dt$ simultaneously increases both the gasdynamic and electromagnetic thrust.

With regards to geometry, it has been concluded that the breech fed thruster is merely the special case $\theta = 180^\circ$ of V-shaped propellants. Exploratory tests with parallel side walls ($\theta = 0^\circ$) have shown it possible to obtain higher thrust/power ratios than with configurations for which $\theta > 0^\circ$. Furthermore, exploratory tests providing propellant from all sides surrounding the plasma, i.e., conical configurations, provide a geometry producing the highest thrust/power ratio.

The ablated propellant mass per discharge has been shown to be a function of the geometry as well as the electrical characteristics of the thruster. Based upon the results of this and previous programs it was possible to formulate an analytic expression for the mass:

$$m_d \propto \frac{A_p}{A_o}\,\frac{E_o}{Z_o} \propto \frac{A_p}{A_o}\int i^2\,dt;\ Z_o = \left(\frac{L_o}{C}\right)^{\frac{1}{2}}$$

which not only successfully correlates available data but also more comprehensively describes recently reported Russian results in terms of the geometry of electrode-

propellant configurations and electrical characteristics.

Previously published results on electrode erosion have also been verified during this program where once again the dependence of electrode erosion on $\int i^2\, dt/m_d$ has been demonstrated. The results obtained in an exploratory attempt to use copper as an electrode material have also been gratifying since it was found that copper eroded only about 10% as much as stainless steel. This result is significant since copper is a much better conductor than stainless steel and the use of copper for electrodes is attractive from that standpoint. as well.

The previously reported correlation of the product of impulse bit and specific impulse as a function of discharge energy has been verified through a dimensional analysis during this program. Furthermore, the efficiency has been shown to be both geometry dependent and dependent upon the non-dimensional Alfvén number through this latter analysis. The increase in efficiency with initial energy could possibly be tied with the magnitude of the Alfvén number as energy is increased but this has not been verified.

The present results are significant in that being able to increase the ratio of thrust to available electric power it has been demonstrated that for the same specific impulse one can achieve higher thruster efficiencies. This is demonstrated by the data presented in Figure 21 where thrust efficiency (η) is plotted as a function of specific impulse (I_s) for the various configurations considered in the past as well as the concepts evaluated during this investigation. Lines of constant T/P have been indicated on this plot and the increase in efficiency at any value of specific impulse is clearly evident as thrust/power is increased. At the present time the only known way to readily move in the direction of increased specific impulse along one of these constant T/P lines is to increase the discharge energy. Hopefully, further research and development programs will lead to other methods for moving in this direction.

Emphasis was not directly placed on optimizing efficiency during this investigation and therefore any comparisons of reported efficiencies with those of other types of thrusters should be made at the same specific impulse.

The V-shaped solid propellant configuration can easily be fed during long time thruster operation. They therefore can be considered practical configurations for space flight applications.

Based upon the limited testing performed, it is concluded that the state-of-the-art of dry (no liquid impregnation) energy storage capacitors for pulsed plasma thruster has not reached the level of reliability of liquid impregnated capacitors when the comparison is made at the same joules/Kg rating.

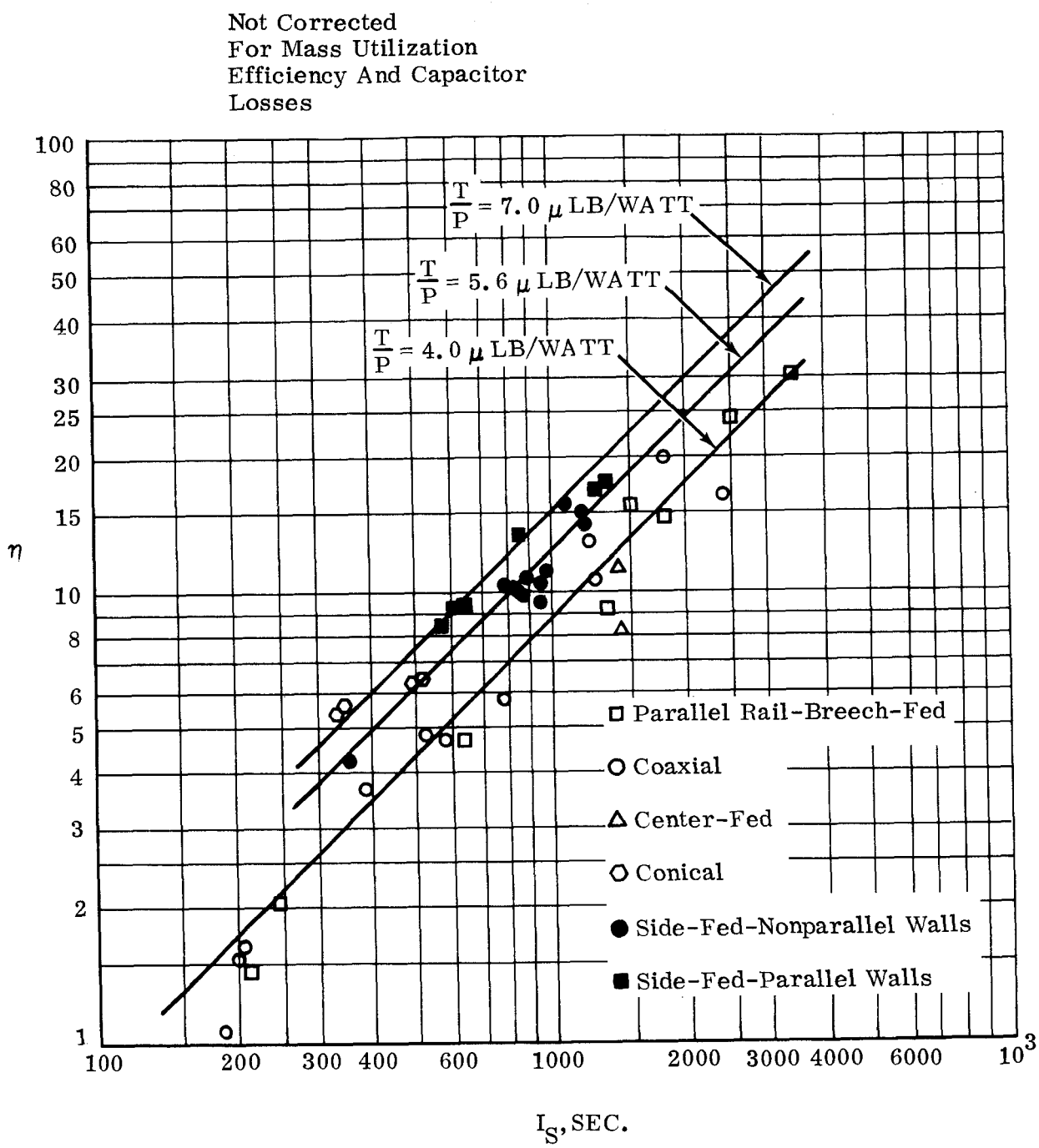

Figure 21. Engine Efficiency as a Function of Specific Impulse

APPENDIX A

ANALYTIC VERIFICATION OF Π_s VERSUS E_o

Previous analytic models which have been formulated with the hope of better understanding the plasma acceleration mechanism have not accurately predicted pulsed plasma thruster performance behavior. A new analytic approach is proposed which thus far has yielded results which are verified by experimental observation.

Our approach, like that of Cheng,[6] centers around the equations of magnetohydrodynamics (MHD). These equations are valid in the macroscopic limit of a continuum and as is well known, one then does not need to concern oneself with the elemental particles composing the plasma, but only with the bulk processes of energy transfer and acceleration of representative conglomerate groups of these particles.

The first step after writing down the MHD equations and corresponding assumptions is nondimensionalization of these equations. The dependent variables appearing in the equations are the plasma density ρ, velocity u, pressure p, and magnetic field intensity B. These are nondimensionalized with respect to characteristic values ρ_o, u_o, $\rho_o u_o^2$ and B_o, respectively. The independent variables are distance, x, and time, t, which are nondimensionalized with respect to some characteristic length ℓ and the characteristic flow time u_o/ℓ.

In their nondimensional form, the MHD equations exhibit three nondimensional parameters - the magnetic Reynold's number R_M, the Alfven number S_o, and the Mach number M_o - defined by the relationships:

$$R_M = \mu_o u_o \ell \sigma$$

$$S_o = \frac{B_o}{\sqrt{2\mu_o \rho_o u_o}}$$

$$M_o = u_o \sqrt{\frac{\rho_o}{\gamma p_o}}$$

where μ_o is the permeability of vacuum, σ is the electrical conductivity, and γ is the ratio of specific heats. A fundamental theorem states that any nontrivial solution to these equations must contain these parameters as arguments.

The basic thruster performance parameter is the impulse bit I. This parameter is the basic parameter, since thrust T and specific impulse I_{sp} are related to it through the following equations:

$$T = fI \tag{A1}$$

$$I_s = \frac{I}{m_d g} \tag{A2}$$

where f is the pulse discharge rate, m_d is the propellant mass used per discharge and g the gravitational acceleration. The thruster efficiency η is given by:

$$\eta = \frac{1}{2g} \frac{T}{P} I_s = \frac{I^2}{2m_d g E_o}$$

where the power $P = fE_o$ and E_o is the discharge energy stored in the capacitor at the time the discharge takes place and is given by $CV^2/2$ with C the capacitance and V the charged voltage applied.

In terms of the macroscopic parameters appearing in the MHD equations, it is well known that the impulse bit is given by:

$$I = A_e \int_o^\infty \left(p + \rho u^2 + \frac{B^2}{2\mu_o} \right) dt$$

where A_e is the area of the plasma cross section at the exit plane of the thruster.

In nondimensional form I may be written,

$$I = A_e \ell \rho_o u_o \int_o^\infty \left(\bar{p} + \bar{\rho} \bar{u}^2 + S_o^2 \bar{B}^2 \right) d\bar{t}$$

where barred quantities are nondimensional. The characteristic impulse bit is therefore $A_e \ell \rho_o u_o$. The next step is to correlate the reference values ρ_o and u_o with the characteristic thruster parameters. If it is assumed that all of the ablated mass is acclerated to a velocity such that its kinetic energy is equal to the discharge energy, the resultant reference velocity u_o will be

$$u_o = \left(\frac{2E_o}{m_d} \right)^{1/2}$$

The density is equal to the mass per unit volume. Let m_d be the mass and let the volume be equal to the volume formed by the propellant-electrode nozzle configuration. Then,

$$\rho_o = \frac{m_d}{V}$$

and,

$$\rho_o u_o = \frac{(2E_o m_d)^{1/2}}{V}$$

Hence,

$$\left(\frac{I}{2E_d m_d} \right)^{1/2} = \frac{A_e \ell}{V} \int_o^\infty \left(\bar{p} + \bar{\rho} \bar{u}^2 + S_o^2 \bar{B}^2 \right) d\bar{t} \qquad \text{(A4)}$$

or equivalently,

$$\eta = \frac{1}{g} \left[\left(\frac{A_e \ell}{V} \right) \int_o^\infty \left(\bar{p} + \bar{\rho} \bar{u}^2 + S_o^2 \bar{B}^2 \right) d\bar{t} \right]^2 \qquad \text{(A5)}$$

Substitution for m_d in terms of the specific impulse via equation (A2) in equation (A4) yields,

$$(\Pi_s) = 2\left(\frac{A_e \ell}{V}\right)^2 E_d \left[\int_o^\infty \bar{p} + \rho \bar{u}^2 + S_o{}^2 \bar{B}^2 \, d\bar{t}\right]^2 \qquad \text{(A6)}$$

Equation (6) verifies the correlation (Figure 9) between the product Π_s and the initial energy. The most important aspect of this plot is the fact that the trend line drawn through our data crosses lines of constant efficiency, indicating that by increasing the discharge energy of a particular thruster the efficiency of that thruster will increase.

The effect of the parameter $(A_e \ell /V)$ in Equation (5) has not yet been fully evaluated, since all thruster configurations that have been considered to date have been limited to values of $(A_e \ell /V)$ between 1 and 2. Since the thrust efficiency is proportional to the square of this term, it is relevant that an attempt should be made to make the latter parameter as large as possible.

APPENDIX B

CAPACITOR EVALUATION TEST

The voltage and current ringout traces obtained when the capacitor was charged using a 10 volt d.c. source are presented below.

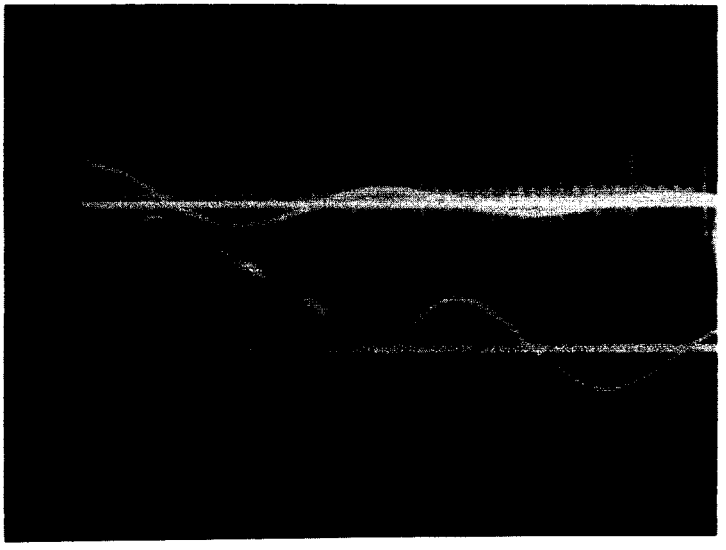

Settings: Upper = Voltage = 5 volts/cm
Lower = Current = .02 volts/cm
Sweep = 2 microseconds/cm

The resistance and inductance can be computed from the equation for an LRC circuit with fixed elements. These equations yield.

$$\omega = 2\pi f = \sqrt{\frac{1}{LC} - \frac{R^2}{4L^2}} \qquad (1)$$

where f is the frequency, L the inductance, R the resistance and C the capacitance. From the current trace, the frequency is found to be $.12162 \times 10^6$ cps. Hence,

$$\omega = .7642 \times 10^6 \text{ cps.}$$

Knowing the ratio of two successive positive or negative current peaks and the time between them we have:

$$R = \frac{2L}{t_2 - t_1} \ln \frac{i_1}{i_2} \qquad (2)$$

Substituting equation (2) for R into equation (1) yields an expression for L in terms of ω and C. Namely,

$$\frac{1}{L} = C \left[\omega^2 + \frac{1}{(t_2 - t_1)^2} \left(\ln \frac{i_1}{i_2} \right)^2 \right]$$

The ratio of the two successive negative peaks is 1.818 and the time between them is 8.22 μ sec. The capacitance is 63 μfd and the inductance is therefore

$$L = 24.93 \text{ nh}$$

Knowing L, R is calculated from equation (2).

$$R = 3.62 \text{ milliohm.}$$

The impedance is given by

$$Z^2 = R^2 + (X_C - X_L)^2$$

where $X_C = 1/\omega C = .02077$ and $X_L = \omega L = .01905$. Thus,

$$Z = 4.0 \text{ milliohm.}$$

The capacitor quality Q is given by $Q = X_C/R = 5.74$

APPENDIX C

MIT SIDEFEED STUDIES

The studies of Vondra and Thomasson[7] became available after completion of this report. Their studies examined in considerable detail, a parallel wall side fed thruster (i.e., the special case $\theta = 0°$). They observe that at fixed energies of either 2 joules or 20 joules the impulse bit amplitude varies with the quantity of propellant mass. This result agrees with the general conclusions reported upon in the main body of this report since one can readily convert the results of Reference 7 in terms of the thrust/power ratio. The variation of efficiency with propellant mass noted in Reference 7 also agrees with earlier findings[1] of solid propellant thrusters whose efficiency was found to correlate with the energy/mass ratio. The suggestion that the performance is partly gasdynamic and partly electromagnetic in origin also agrees with earlier studies and the conclusion of the present study. It should be noted, however, that by demonstrating the dependence of m_d on the integral of the current squared and electrode-propellant configuration during our latest study it is questionable as to whether observed increases in thrust/power with mass are strictly gasdynamic in origin. Since the contribution to the impulse bit through magnetic pressure forces is also proportional to this integral as well as a geometric factor, it is clear that both contributions are amplified by increasing the integral of current squared. To resolve the question as to which contribution produces the largest effect on thrust/power would require knowledge of the magnetic field as a function of time at the breech and exit planes as well as knowledge of the total energy absorbed by the plasma during the discharge.

APPENDIX D
GASDYNAMIC CONSIDERATIONS OF THRUST-TO-POWER

In Section 4.4 of this report it was pointed out that simple gasdynamics theory predicts a dependence of the thrust/power ratio (T/P) on the square root of the mass to energy ratio $(m_d/E_o)^{\frac{1}{2}}$. Therefore, one might expect a correlation between these two latter parameters if the thruster behaved purely as a gasdynamic device. Figure 23 presents available thrust/power data as a function of the mass/energy ratio. Unlike the correlation observed in Figure 10, no general correlation of the data is observed in Figure 23. The lack of correlation of most of the data in Figure 23 is attributed to the existence of an electromagnetic contribution to the impulse bit, not accounted for in the gasdynamic analysis leading to Equation 2, thus supporting the hypothesis that the impulse bit of the pulsed ablative thruster, is both gasdynamic and electromagnetic in origin. It is interesting to note, however, that the cylindrical data of Ref. 2 does appear to correlate in accordance with gasdynamic predictions. This observation is perhaps due to the fact that magnetic pressure forces in the latter cylindrical configuration are radially inward directed in a non-thrust producing direction.

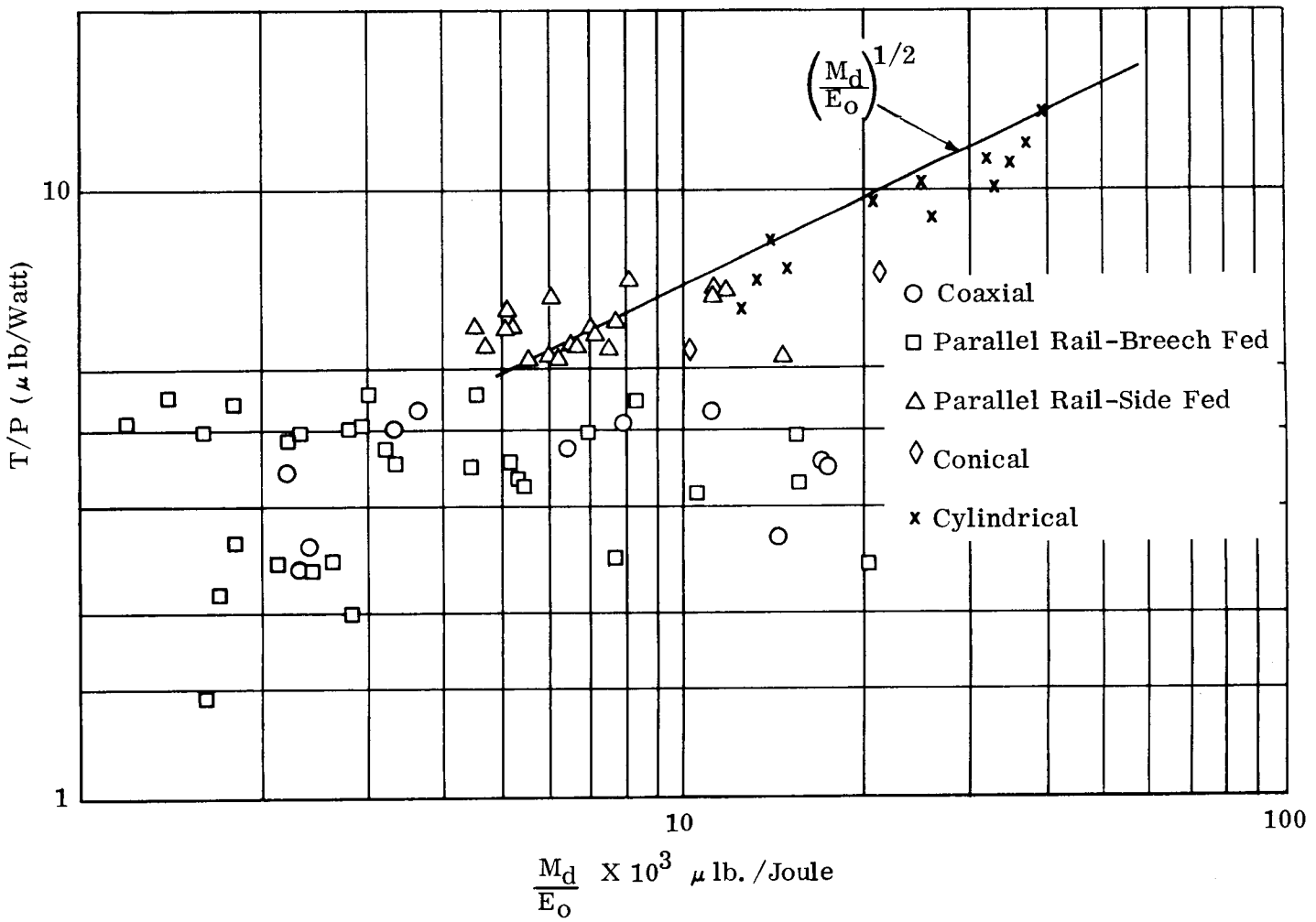

Figure 23. Thrust-to-Power as a Function of Mass to Energy Ratio

REFERENCES

1. Guman, W., Quasi-steady and Short Pulse Discharge Thruster Experiments, NASA CR 111935, Final Technical Report, PCD-TR-71-3, FHR 3795-1, PC004R7001, Fairchild Industries, Farmingdale, N.Y., June, 1971

2. Solbes, A., Personal Communication, 12/2/71, Massachusetts Institute of Technology, Cambridge, Massachusetts, Dept. of Aeronautics and Astronautics.

3. Guman, W., Switch-Triggered Pulsed Plasma Accelerator Thrust Measurements, AIAA Journal, June, 1965, p. 1158, Vol. 3, No. 6, June, 1965,

4. Popov, N.P., Vereshchagin, V.L., Study of the Erosion of a Dielectric in a Conical Plasma Accelerator, Samoletostroenie i Tekhnika Vozdushnogo Floto, No. 20., 1970, Available as IAA A71-14597.

5. Malliaris, A.C., Jahn, R.R., Garrison, R.L., Libby, D.R., Quasi-steady MPD Propulsion at High Power NASA CR 111872, Final Technical Report AVSO-0146-71-RR, AVCO Corp., Wilmington, Massachusetts, Feb., 1971.

6. Cheng, D.Y., Application of a Deflagration Plasma Gun as a Space Propulsion Thruster, AIAA Journal, Vol. 9, No. 9, Sept. 1971, p. 1681.

7. Vondra, R.J., Thomassen, K.I., Performance Improvements in Solid Fuel Microthrusters, AIAA 10th Aerospace Sciences Meeting, San Diego, California, AIAA Paper 72-210, Jan. 1972.

NASA CR-112035

DISTRIBUTION LIST
NAS1-10944

	No. Copies
NASA Langley Research Center Hampton, VA 23365	
Attn: Program Reports & Analysis Unit, Mail Stop 122	1
Raymond L. Zavasky, Mail Stop 110	1
James M. Hoell, Mail Stop 160	10
Technology Utilization Office, Mail Stop 139A	1
NASA Ames Research Center Moffett Field, CA 94035	
Attn: Library, Mail Stop 202-3	1
NASA Flight Research Center P. O. Box 273 Edwards, CA 93523	
Attn: Library	1
Jet Propulsion Laboratory 4800 Oak Grove Drive Pasadena, CA 91103	
Attn: Library, Mail 111-113	1
Dr. Noble M. Nerheim, Mail 122-123	1
NASA Manned Spacecraft Center 2101 Webster Seabrook Road Houston, TX 77058	
Attn: Library, Code JM6	1
NASA Marshall Space Flight Center Huntsville, AL 35812	
Attn: Library	1
Ernst Stuhlinger, AD-S	1
NASA Lewis Research Center 21000 Brookpark Road Cleveland, OH 44135	
Attn: Library, Mail Stop 60-3	1
Wolfgang E. Moeckel, Mail Stop 301-1	1
George R. Seikel, Mail Stop 301-1	1
MASA Goddard Space Flight Center Greenbelt, MD 20771	
Attn: Library	1
William C. Isley, Code 730	1
Robert A. Collens, Code 734	1
John F. Kennedy Space Center Kennedy Space Center, FL 32899	
Attn: Library, Code IS-DOC-12L	1
National Aeronautics & Space Administration Washington, DC 20546	
Attn: Library, Code KSS-10	1
NASA Code RP	1
James Lazar, Code KSS-10	1
Jerome P. Mullin, Code RPE	1
Joseph R. Burke, Code SC	1

NASA CR-112035

DISTRIBUTION LIST
NAS1-10944

	No. Copies
COMSAT Laboratories Positioning & Orientation Branch Box 115 Clarksburg, MD 20734	
Attn: Bernard Free	1
George Huson	1
Princeton University Guggenheim Laboratories James Forrestal Campus Princeton, NJ 08540	
Attn: Woldemar F. von Jaskowsky	1
TRW Systems Inc. One Space Park Redondo Beach, CA 90278	
Attn: Dr. C. L. Dailey	1
Air Force Weapons Laboratory Kirtland Air Force Base, NM 87417	
Attn: WLPC/Capt. C. F. Ellis	1
Thermal Mechanical Research Laboratory OAR USAF Wright Patterson Air Force Base, OH 45433	
Attn: Eric Soehngen	1
General Electric Company Missile & Space Division Space Sciences Laboratory P. O. Box 8555 Philadelphia, PA 19101	
Attn: Dr. Thomas W. Karras	1
Los Alamos Scientific Laboratories P. O. Box 1663 Los Alamos, NM 87544	
Attn: Dr. Stratton	1
University of California, San Diego LaJolla, CA 92037	
Attn: Professor R. Lovberg	1
United States Air Force Office of Scientific Research Washington, DC 20025	
Attn: M. Slawsky	1
Princeton University Forrestal Research Center Princeton, NJ 08540	
Attn: Dr. R. G. Jahn	1

DISTRIBUTION LIST
NAS1-10944

	No. Copies
Giannini Scientific Corporation 3839 South Main Street Santa Ana, CA 92702 Attn: Adriano Ducati	1
Naval Research Laboratory Washington, DC 20390 Attn: R. T. Beal, Code 7973	1
Air Force Rocket Propulsion Laboratory Edwards, CA 93523	
Attn: Walter Detgen, Code LKD	1
Dr. Clark Hawk, Code LKD	1
Thomas Waddel, Code LKD	1
Lt. Stanley Rosen, Code LKD	1
Wright-Patterson Air Force Base, OH 45433 Attn: Dr. Fritts, AFAPL/POD	1
Andrews Air Force Base, MD 20331 Attn: Lt. Col. James Nelson, AFSC/DLTP	1
Headquarters United States Air Force Washington, DC 20330 Attn: Lt. Col. R. Wolfsberger/RDSD	1
Air Force Unit Post Office Los Angeles, CA 90045 Attn: Lt. Craig Baer, SAMSO/SYAS	1
Massachusetts Institute of Technology Lincoln Laboratories Lexington, MA 02173	
Attn: Dr. Robert Vondra	1
Donal McClellen	1
Massachusetts Institute of Technology Cambridge, MA 02139	
Attn: Dr. Albert Solbes	1
Dr. Keith Thomassen	1
Aerospace Corporation P. O. Box 95058 Los Angeles, CA 90045 Attn: Robert Doebler, BA2, Rm 2068	1
RCA Astro Electronics Division P. O. Box 800 Princeton, NJ 08540 Attn: Dan Balzer	1
Johns Hopkins University Applied Physics Laboratory 8621 Georgia Avenue Silver Spring, MD 20910 Attn: Robert E. Fishell	1

NASA CR-112035

DISTRIBUTION LIST
NAS1-10944

	No. Copies
Department of the Navy Strategic Systems Project Office Washington, DC 20390 Attn: Gerald Hoskins	1
Johns Hopkins University Applied Physics Laboratory 8621 Georgia Avenue Silver Spring, MD 20910 Attn: James Samola	1
Jet Propulsion Laboratory Guidance & Control Section 4800 Oak Grove Drive Pasadena, CA 91103	
Attn: W. E. Bachman	1
Franseco Roselli-Lorengini	1
John B. Dahlgren	1
NASA Scientific & Technical Information Facility P. O. Box 33 College Park, MD 20740	10 plus reproducib